Global Biogeochemical Cycles

RESEARCH ARTICLE
10.1029/2024GB008342

Multi-Elemental Tracers in the Amerasian Basin Reveal Interlinked Biogeochemical and Physical Processes in the Arctic Ocean Upper Halocline

L. M. Whitmore[1], L. Jensen[2], J. Granger[3], Y. Xiang[4], L. Kipp[5], A. Pasqualini[6], R. Newton[7], A. M. Agather[8], R. F. Anderson[9], E. E. Black[10], K. L. Bowman[11], A. Bourbonnais[12], M. A. Brzezinski[13], R. M. Bundy[2], M. A. Charette[14], R. L. Edwards[15], J. N. Fitzsimmons[16], D. A. Hansell[17], P. J. Lam[11], P. Morton[16], M. A. Saito[14], P. Schlosser[6], A. M. Shiller[18], W. M. Smethie[9], B. S. Twining[19], R. J. Woosley[20], and R. Zhang[21]

[1]International Arctic Research Center, University of Alaska Fairbanks, Fairbanks, AK, USA, [2]Applied Physics Laboratory, University of Washington, Seattle, WA, USA, [3]University of Connecticut, Groton, CT, USA, [4]Louisiana State University, Baton Rouge, LA, USA, [5]Rowan University, Glassboro, NJ, USA, [6]Arizona State University, Tempe, AZ, USA, [7]Columbia University, New York City, NY, USA, [8]Science and Technology Corporation, Hampton, VA, USA, [9]Lamont-Doherty Earth Observatory of Columbia University, New York City, NY, USA, [10]University of Rochester, Rochester, NY, USA, [11]University of California Santa Cruz, Santa Cruz, CA, USA, [12]School of the Earth, Ocean, and Environment, University of South Carolina, Columbia, SC, USA, [13]University of California, Santa Barbara, CA, USA, [14]Marine Chemistry and Geochemistry Department, Woods Hole Oceanographic Institution, Woods Hole, MA, USA, [15]Department of Geology and Geophysics, University of Minnesota, Minneapolis, MN, USA, [16]Department of Oceanography, Texas A&M University, College Station, TX, USA, [17]University of Miami, Miami, FL, USA, [18]Daylight Geochemical, L.L.C, Slidell, LA, USA, [19]Bigelow Laboratory for Ocean Science, East Boothbay, ME, USA, [20]Massachusetts Institute of Technology, Cambridge, MA, USA, [21]Shanghai Jiao Tong University, Shanghai, China

Abstract The physical and biogeochemical properties of the western Arctic Ocean are rapidly changing, resulting in cascading shifts to the local ecosystems. The nutrient-rich Pacific water inflow to the Arctic through the Bering Strait is modified on the Chukchi and East Siberian shelves by brine rejection during sea ice formation, resulting in a strong halocline (called the Upper Halocline Layer (UHL)) that separates the cold and relatively fresh surface layer from the warmer and more saline (and nutrient-poor) Atlantic-derived water below. Biogeochemical signals entrained into the UHL result from Pacific Waters modified by sediment and river influence on the shelf. In this synthesis, we bring together data from the 2015 Arctic U.S. GEOTRACES program to implement a multi-tracer (dissolved and particulate trace elements, radioactive and stable isotopes, macronutrients, and dissolved gas/atmospheric tracers) approach to assess the relative influence of shelf sediments, rivers, and Pacific seawater contribution to the Amerasian Arctic halocline. For each element, we characterized their behavior as mixing dominated (e.g., dCu, dGa), shelf-influenced (e.g., dFe, dZn), or a combination of both (e.g., dBa, dNi). Leveraging this framework, we assessed sources and sinks contributing to elemental distributions: shelf sediments (e.g., dFe, dZn, dCd, dHg), riverine sources, (e.g., dCu, dBa, dissolved organic carbon), and scavenging by particles originating on the shelf (e.g., dFe, dMn, dV, etc.). Additionally, synthesized results from isotopic and atmospheric tracers yielded tracer age estimates for the Upper Halocline ranging between 1 and 2 decades on a spatial gradient consistent with cyclonic circulation.

Key Points:

- Chemical tracer relationships to salinity help define the role of Pacific water, rivers, sediments on the biogeochemistry of the halocline
- Dissolved Mn, V, Cd, Cu, Cd and Co are scavenged by MnO_2; scavenging in the halocline is likely an important sink for these constituents
- Age of halocline waters (10–20 years) is consistent with circulation of the Beaufort Gyre

Supporting Information:

Supporting Information may be found in the online version of this article.

Correspondence to:

L. M. Whitmore and L. Jensen,
lmwhitmore@alaska.edu;
jensenla@uw.edu

Citation:

Whitmore, L. M., Jensen, L., Granger, J., Xiang, Y., Kipp, L., Pasqualini, A., et al. (2025). Multi-elemental tracers in the Amerasian Basin reveal interlinked biogeochemical and physical processes in the arctic ocean upper halocline. *Global Biogeochemical Cycles*, *39*, e2024GB008342. https://doi.org/10.1029/2024GB008342

Received 16 SEP 2024
Accepted 11 MAR 2025

Author Contributions:

Conceptualization: L. M. Whitmore, L. Jensen, J. Granger
Data curation: L. M. Whitmore, L. Jensen, J. Granger, Y. Xiang, L. Kipp, A. Pasqualini, A. M. Agather, R. F. Anderson, E. E. Black, K. L. Bowman, A. Bourbonnais, M. A. Brzezinski, R. M. Bundy, D. A. Hansell, P. Morton, P. Schlosser, W. M. Smethie, R. J. Woosley, R. Zhang
Funding acquisition: R. F. Anderson
Investigation: L. M. Whitmore, L. Jensen, J. Granger, Y. Xiang, L. Kipp, A. Pasqualini, R. Newton, E. E. Black

1. Introduction

The surface air temperature over the Arctic is warming between two and four times faster than the planetary average (Masson-Delmotte et al., 2021; Rantanen et al., 2022; Serreze et al., 2009). The impact on the Arctic cryosphere, including the sea-ice cover, land snow and ice, and permafrost, is already significant, and there is no reason to believe that current trends will slow in the near future (Stroeve et al., 2025). The Arctic Ocean connects the Pacific and Atlantic Oceans, promoting the exchange of heat and salt, with local implications for sea ice cover (Polyakov et al., 2017) and global implications for meridional overturning circulation (Aagaard & Carmack, 1994). Cold and relatively fresh Pacific Ocean-derived water flows through the Bering Strait between Alaska and Russia, sitting above warmer, more saline Atlantic Ocean-derived water flowing through the Fram Strait and Barents Sea. Pacific waters also carry different biogeochemical signals (such as lower oxygen and higher macronutrients and trace metals) compared to Atlantic waters, creating strong vertical biogeochemical

Methodology: L. M. Whitmore, L. Jensen, Y. Xiang, L. Kipp, A. Pasqualini
Visualization: L. M. Whitmore, L. Jensen, J. Granger, Y. Xiang, L. Kipp, A. Pasqualini, E. E. Black
Writing – original draft: L. M. Whitmore, L. Jensen, J. Granger, Y. Xiang, L. Kipp, A. Pasqualini, R. Newton
Writing – review & editing: L. M. Whitmore, L. Jensen, J. Granger, Y. Xiang, L. Kipp, A. Pasqualini, R. Newton, A. M. Agather, R. F. Anderson, E. E. Black, K. L. Bowman, A. Bourbonnais, M. A. Brzezinski, R. M. Bundy, M. A. Charette, R. L. Edwards, J. N. Fitzsimmons, D. A. Hansell, P. J. Lam, P. Morton, M. A. Saito, P. Schlosser, A. M. Shiller, W. M. Smethie, B. S. Twining, R. J. Woosley, R. Zhang

gradients during physical mixing between the two water types (Jones et al., 1998). The fresh, river-influenced Pacific inflow through the Bering Strait results in a strong salinity gradient ("halocline") between the surface to ~300 m in the Amerasian Basin. This prominent halocline stands out as a defining feature of the Amerasian Basin, resulting in stratification that both impedes the delivery of heat and prevents significant mixing from underlying Atlantic water (AW) to the sea surface (Aagaard et al., 1981).

The Amerasian Basin halocline, hereafter referred to as the Upper Halocline Layer (UHL), is further distinguished by its association with a sharply defined nutrient maximum in Pacific-derived water masses (Figure 1; Anderson et al., 2013; Jones & Anderson, 1986). Nutrient concentrations are high, relative to Atlantic-derived waters, in Pacific inflow through Bering Strait (Bering Strait Inflow (BSI)) and they are further increased by regeneration and brine rejection in cold, saline shelf bottom waters (Cooper et al., 2005; Granger et al., 2018). This nutrient maximum is advected offshore at depths between roughly 50 and 300 m, but is suppressed from upwelling to the surface by stratification due to large surface freshwater inputs (Anderson et al., 2013; Granger et al., 2018; Jones & Anderson, 1986; Moore et al., 1983). The nutrient maximum is observed in the Canada and Makarov Basins, the western edge of Fram Strait discharging into the Nordic Seas, and permeates the Canadian Arctic Archipelago (CAA) into Baffin Bay, exiting through the Davis Strait into the Labrador Sea (Codispoti & Owens, 1975; Dodd et al., 2012; Jones & Coote, 1980; Jones et al., 2003; Lehmann et al., 2019).

The evolution of nutrients and tracers in the Canada and Makarov Basins provides insights into processes contributing to their modifications, their influence on regional biogeochemistry, and their ultimate fate in the Arctic Ocean. Recent GEOTRACES efforts in the Arctic Ocean basins have also revealed distinctive trace element and isotopologue distributions coincident with the Amerasian Basin halocline nutrient maximum. Some trace elements are elevated within the halocline (e.g., dissolved iron, zinc, cadmium, and radium; see Section 4, Table 1; Colombo et al., 2020; Jensen et al., 2019; Kipp et al., 2019; Zhang et al., 2019), whereas others are unexpectedly low (e.g., dissolved vanadium; Whitmore et al., 2019) relative to predicted concentrations based on conservative mixing of Pacific, Atlantic, and riverine water. Furthermore, some tracers appear to be conserved in the halocline and may even be evident downstream at the Arctic Ocean outflow sites (e.g., dissolved organic carbon (DOC); Mathis et al., 2005), while others are influenced by internal cycling (Anderson et al., 2010; Colombo et al., 2019; Jones et al., 2003; Lehmann et al., 2019; Taylor et al., 2003).

The physical properties of the UHL derive from the interaction of source waters, including Pacific inflow, and brine rejection during sea ice formation over the shelves (Anderson et al., 2013), which cannot be deconvolved with temperature and salinity alone. Geochemical tracer distributions (e.g., radium, nitrate isotopes, and manganese particles) suggest an important role of shelf processes and riverine input in modifying tracers during transit from the Pacific Ocean across the shallow Bering and Chukchi Sea shelves. These insights improve our understanding of mechanisms behind important physical processes such as stratification, heat transport, and biogeochemical processes such as the carbon cycle, in the upper layers of the Arctic Ocean.

In light of rapid environmental change, it is imperative to synthesize the current biogeochemistry of the Arctic Ocean. To this end, recent GEOTRACES expeditions have resulted in a quasi-synoptic survey of geochemical tracers spanning the Arctic Ocean, including the Pacific-influenced Amerasian Basin. We examine the distributions of trace elements and isotopes (TEIs) to investigate the transformation of Pacific-origin waters into those observed in the UHL. We also explore geochemical tracer applications for water mass age, trace metal scavenging in the upper water column, and identification of shelf sources contributing to the cold halocline. Lastly, we consider how anticipated environmental changes are likely to modify the geochemistry of the halocline and the consequences for the Arctic Ocean ecosystem. Our analysis highlights the disproportionate influence of shelf dynamics and lateral advection on basin geochemical properties. Changes in the physical and biological regimes are likely to lead to significant modifications in the distributions of geochemical tracers.

1.1. Physical, Biogeochemical, and Geographic Setting

The Amerasian Basin (Figure 1) is separated from the Eurasian Basin by the Lomonosov Ridge (sill depth ~1,500 m) and is further divided into the Makarov and Canada Basins by the Alpha-Mendeleev Ridge (~2500 m, not shown in Figure 1). The Amerasian Basin is flanked by the expansive East Siberian and Chukchi Seas, and the narrower Beaufort Sea shelf. To the east, it is bordered by the shallower CAA, a vast network of passageways and shelf seas (See Figure 1a and numerical legend for geographic context).

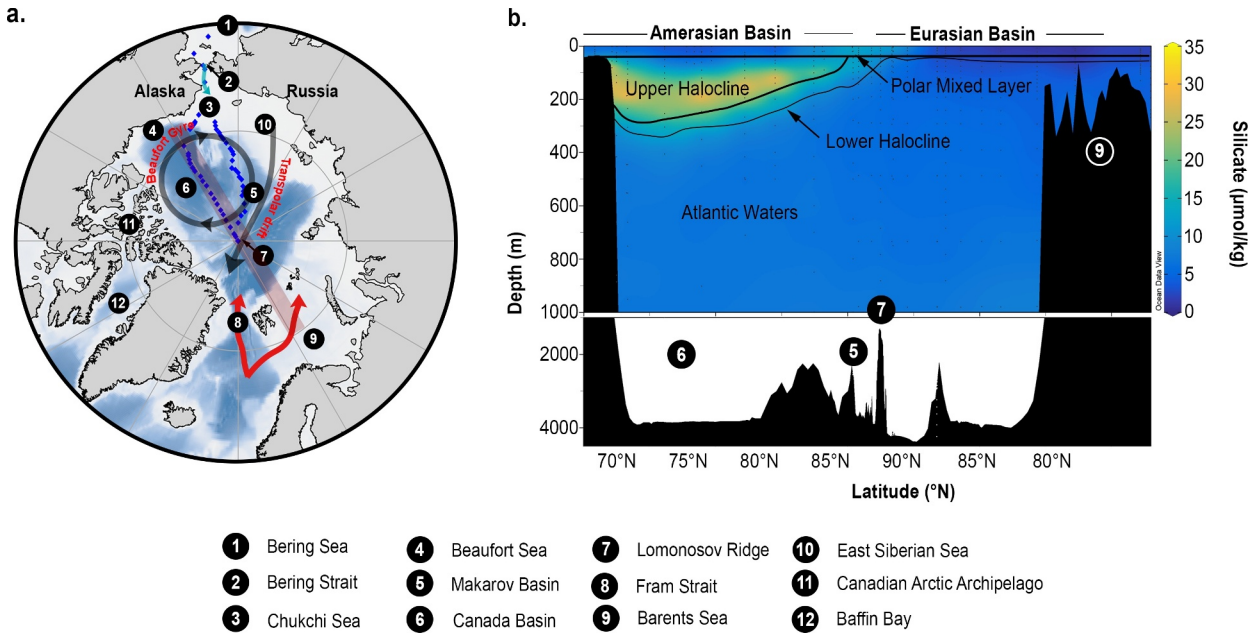

Figure 1. (a) The geography of the Arctic Ocean with features labeled as numbers and defined in the legend. General bathymetry of the basin is represented by the color gradient (light blue to dark blue) from light blue (shelves) to dark blue (deep basins). Major circulation of seawater is depicted by arrows in light blue (Pacific inflow), black (surface circulation of the Beaufort Gyre and Transpolar Drift), and red (Atlantic inflow). Blue diamonds indicate the station locations utilized in this study (2015 US GEOTRACES transect, GN01). The hydrography of the Arctic Ocean is depicted in figure (b); the section shown is indicated by the shaded red rectangle. This study investigates the upper halocline layer (UHL) in the Amerasian sector of the ocean, noted for its characteristic maximum in silicate (*z*-axis). The data from this study only includes the upper 1,000 m of the water column and (b) has been divided into two panels: the upper 1,000 m and the waters deeper than 1,000 m; both panels have linear depth axes. However, the bottom sub-plot in (b) is solely for bathymetric reference and has been compressed vertically relative to the upper 1,000 m. Modified from Whitmore et al., 2019; silicate data is from GEOTRACES Intermediate Data Product Group, 2021 and van Ooijen et al., 2016.

Density gradients in the Arctic Ocean are dominated by salinity. The surface waters, that is, the Polar Mixed Layer (PML), are among the freshest in the world ocean because of large influxes of river runoff, seasonal sea-ice melt, and precipitation. The PML extends from the surface to ~50 m. Slightly more saline waters make up the UHL, including nutrient-poor Alaskan Coastal Water (ACW; S: 30–32 in the Canada Basin only), Pacific Summer Water (PSW; S: 32–33), and Pacific Winter Water (PWW; S: 33–33.5). PSW and PWW are Pacific-origin waters modified by physical and biogeochemical seasonal processes occurring over the Pacific Arctic shelf seas (see Section 4). PWW is formed on the Bering and Chukchi shelves in winter as a result of cooling and salination during sea ice formation and subsequent brine rejection (Shimada et al., 2005; Woodgate, Aagaard, Swift, et al., 2005). All three water masses (ACW, PSW, and PWW) ventilate the UHL via bathymetric features, including the Herald and Barrow Canyons (Figure 3). These waters move from the boundaries into the basin along isopycnal surfaces and in eddies that frequently form in the shelf break jet and slope currents, which tend to travel parallel to the shelf break (Corlett & Pickart, 2017; Pickart et al., 2005; Spall et al., 2008; Steele et al., 2004, p. 200).

Table 1
Sub-Basin-Scale Age Estimates of the Upper Halocline Layer (UHL) Derived From SF_6, $^3H/^3He$, and $^{228}Ra/^{226}Ra$

Tracer	Input	Mendeleev ridge Makarov basin Age (yr)	Canada basin (77–84°N) Age (yr)	S. Canada basin (<77°N) Age (yr)
SF_6[a]	Atmosphere (anthropogenic)	~9–16	11–16	~16–19
$^3H/^3He$[b]	Atmosphere, river runoff (anthropogenic, natural radioactive decay)	6–14	10–18	14–23
$^{228}Ra/^{226}Ra$[b]	Sediment (natural radioactive decay)	7–9	8–14	13–17

[a](Smethie & Swift, 2018; Swift et al., 2016). [b]This Study.

The export of water masses and associated shelf-derived elements into the halocline via the shelf break jet exhibits seasonal variability and is additionally correlated with climate forcings on an interannual time scale. The export of sediment-derived materials from the shallow Chukchi shelf (~50 m) via the shelf break jet is strongest in the fall and winter (Kipp et al., 2020). PWW is the dominant water mass carried in both of these currents, with newly-ventilated PWW most prevalent between March and August in the slope current and between mid-May and mid-September along the shelf break, while remnant PWW was dominant the rest of the year (M. Li et al., 2019).

Benthic inputs from sediments are enhanced during PWW formation due to convective mixing resulting from sea ice formation. The PWW that reaches the shelf break jet in the fall and winter (which was farther south on the shelf at the time of PWW formation) has therefore had a longer contact time with shelf sediments to become enriched in sediment-derived elements (Kipp et al., 2020; Kondo et al., 2016; Mathis et al., 2007). Because the 2015 U.S. GEOTRACES transect took place in the late summer and fall, the concentrations of sediment-derived elements along the Chukchi slope may represent seasonal maxima, though the distribution of non-conservative elements may also be influenced by biological uptake and/or particle adsorption during transport across the shelf, resulting in lower concentrations.

2. Data Used in This Study

This paper investigates the UHL, leveraging observations from the Amerasian Basin (Figure 1). Geochemical trace element and isotope (TEI) data used in this study are available in the GEOTRACES Intermediate Data Product (IDP) 2021 (GEOTRACES Intermediate Data Product Group, 2021). This study focuses on data from the upper 1,000 m of the water column from the 2015 U.S. GEOTRACES Arctic expedition (GN01). Additional hydrochemical parameters, such as nutrients and carbon, are available at the "CLIVAR and Carbon Hydrographic Data Office" (https://cchdo.ucsd.edu/). Hydrographic sampling occurred following GO-SHIP methodology (Hood et al., 2010). Trace metal clean sampling adhered to GEOTRACES approved methods (Cutter et al., 2014). Some parameters synthesized herein have been published in project-specific publications; our goal is to compare and contrast the tracers in one study to identify patterns in tracer behavior.

The data in this study were extracted from three types of sampling systems: standard rosette, trace metal clean rosette, and large volume in situ filtration (McLane Pumps). Depths of sampling between the systems may not have been the same; to match depths, the Conductivity, Temperature, and Depth (CTD) profile was binned to 5 m (e.g., 2.5, 7.5, 12.5, etc.). Water samples were assigned to the nearest 5 m bin. A few parameters (macronutrients, SF6-derived age, suspended particulate material, and fraction of Mn oxides (MnO_2)) were linearly interpolated to all bins to allow for comparison to all other parameters.

Data availability, including sampling methods and analytical methods, are reported in (Table 2). In this paper, we adopt a shorthand nomenclature to indicate element (E) type: dE (dissolved), pE (particle), dE_L (dissolved labile fraction). The abbreviations used in this manuscript are fully articulated in Table 3.

3. Age Tracers in the Amerasian Halocline

Transient chemical tracers can be used to determine when the waters in the halocline were last in contact with the atmosphere or shelf sediments, providing estimates of ventilation timescales or the apparent "age" of water since detraining from the continental shelf. Together, tracers from the GN01 transect provide evidence that the Makarov Basin was ventilated more recently than the Canada Basin and the oldest water in the Upper Halocline resides in the southern part of the Canada Basin.

Specifically, chlorofluorocarbons (CFCs) and sulfur hexafluoride (SF_6) are chemically stable anthropogenically-sourced gasses with well-known source functions that enter the surface ocean through air-sea gas exchange (Fine, 2011) and are subsequently subducted into the halocline. Comparing their halocline concentrations to the known history of atmospheric concentrations (Bullister & Warner, 2017) can provide an estimate of the time elapsed since the water was in contact with the atmosphere over the shelf for time scales of about 1–70 years for CFCs and 1–50 years for SF_6 (with typical errors of 2%–4%). The ratio of tritium (^3H) and helium-3 (^3He) can be applied in a similar manner. Tritium is naturally produced by the interaction of cosmic rays with oxygen and nitrogen and decays into ^3He with a half-life of 12.32 ± 0.02 years (Lucas & Unterweger, 2000). Nuclear weapons testing in the 1960s also created an anthropogenic release of tritium that was several orders of magnitude larger than the natural background level. In the atmosphere, tritium quickly oxidizes, enters the hydrological cycle, and

Table 2
Data Availability and Methods

Parameter	Data repository	Sampling methods	Analytical methods
dMn, dFe, dNi, dCu, dZn, dCd	IDP[a]	GEOTRACES Cookbook: Cutter et al., 2014	Jensen, Wyatt, et al., 2020
dV, dGa, dBa	IDP[a]	GEOTRACES Cookbook: Cutter et al., 2014	Whitmore et al., 2019, 2020, 2022
dCH_4	BCO-DMO[b]	Roberts & Shiller, 2015	Roberts & Shiller, 2015
Ra isotopes	IDP[a]	GEOTRACES Cookbook: Cutter et al., 2014	Kipp et al., 2019
DIC, TA, pH_{sws}	CCHDO[c]	Dickson et al., 2007	Dickson et al., 2007; Carter et al., 2013
DOC	IDP	GEOTRACES Cookbook: Cutter et al., 2014	Halewood et al., 2022
^{230}Th, ^{231}Pa	IDP[a]	GEOTRACES Cookbook: Cutter et al., 2014	Anderson et al., 2012
^{3}H, ^{3}He	EarthChem Library[d]	Ludin et al., 1997	Ludin et al., 1997
Hg	IDP[a]	Lamborg et al., 2012	Agather et al., 2019
Nitrous oxide concentrations and stable isotopes	Arctic Data Center[e]	Bourbonnais et al., 2017, 2023	Bourbonnais et al., 2017, 2023
CFC-11, CFC-12, SF_6	IDP[a]	GO-SHIP Repeat Hydrography Manual	Hood et al., 2010
pMn, pFe, pCo, pNi, pCu, pZn, pBa, pCd (total and labile), (bottle)	BCO-DMO[f]	GEOTRACES Cookbook: Cutter et al., 2014	Ohnemus et al., 2017; Twining et al., 2019
Major particle composition (pump)	IDP[a]	GEOTRACES Cookbook: Cutter et al., 2014	Xiang & Lam, 2020

[a]GEOTRACES Intermediate Data Product Group, 2021. [b]Whitmore & Shiller, 2024. [c]CCHDO Hydrographic Data Office, 2023. [d]Schlosser et al., 2023. [e]Bourbonnais & Altabet, 2021. [f]Twining et al., 2019.

is deposited to the ocean via precipitation, continental runoff, and vapor exchange (Weiss & Roether, 1980). $^{3}H/^{3}He$ dating utilizes the principle that the ^{3}He accumulation in subsurface waters is a proxy for the time elapsed since that water parcel last equilibrated with the atmosphere (Jenkins & Clarke, 1976). $^{3}H/^{3}He$ ages are appropriate for water masses and processes with timescales from months to ca. 60 years. Typical errors on the apparent $^{3}H/^{3}He$ ages in the halocline layer are 2%–3%.

While these atmospherically sourced tracers provide estimates of when the halocline water was last at the surface, radium isotopes can provide information on the time elapsed since water was last in contact with shelf sediments. Radium is produced through the decay of thorium in shelf sediments and is soluble in seawater. The half-life of radium-228 (^{228}Ra; $t_{1/2}$ = 5.75 years) is ideal for determination of ages in the halocline since it has a residence time of less than 30 years. Normalizing ^{228}Ra to the longer-lived radium-226 (^{226}Ra; $t_{1/2}$ = 1,600 years) corrects for any dilution or mixing during transit so that any decrease in the ratio is due to ^{228}Ra decay.

Along the GN01 transect, the concentrations of CFCs and SF_6 indicate that the waters sampled in the halocline were last at the surface ∼1–2 decades ago (Smethie & Swift, 2018; Swift et al., 2016). This timescale is similar to upper halocline $^{3}H/^{3}He$ apparent ages in the Amerasian Basin, which range from 5 to 23 years. These values are also in line with previously published mean residence times based on $^{3}H/^{3}He$ (e.g., Ekwurzel et al., 2001; Schlosser et al., 1999), with the upper limit being ∼5 years higher. Kipp et al. (2019) determined that the Canada Basin halocline is ventilated with Chukchi shelf inputs on timescales <19–23 years with the $^{228}Ra/^{226}Ra$ ratio method, demonstrating consistency between tracers. The SF_6, $^{228}Ra/^{226}Ra$, and $^{3}H/^{3}He$ estimates from 2015 align well with ages based on $^{3}H/^{3}He$ measurements collected in this region over a period of 27 years (1987–2013; Pasqualini et al., 2024).

Table 3
Acronyms Used Throughout the Manuscript

Acronym	Meaning
ACW	*Alaskan Coastal Water*
AW	*Atlantic Water*
AOU	*Apparent oxygen utilization*
CAA	*Canadian Arctic Archipelago*
CTD	*Conductivity Temperature Depth profiler*
BSI	*Bering Strait Inflow*
δ	*(delta) Anomaly in per mil*
dE	*Dissolved fraction of element E*
DIC	*Dissolved inorganic carbon*
DOC	*Dissolved organic carbon*
DOM	*Dissolved organic matter*
E	*An element of interest*
IDP	*Intermediate Data Product*
*N**	*Nitrogen deficit from predicted stoichiometries where* $N^* = ([NO3] - 16 * [PO4] + 2.9) * 0.87$
pE	*Particulate fraction of element E*
PML	*Polar mixed layer*
POC	*Particulate organic carbon*
PSW	*Pacific summer water*
PWW	*Pacific winter water*
SIZ	*Seasonal ice zone*
SPM	*Suspended particulate matter*
TEIs	*Trace elements and isotopes*
UHL	*Upper halocline layer*

The episodic nature of shelf outflows (e.g., via eddies and brine rejection), along with inputs from multiple shelves (e.g., Chukchi, East Siberian) results in heterogeneity in the halocline. It is therefore useful to consider ventilation timescales on a smaller spatial resolution when interpreting the distribution of elements in the halocline on basin-wide scales. Ages in the UHL (centered on σ_Θ 26.5 kg m^{-3}) on the GN01 transect indicate that the youngest waters were located on the 180ºW section above the Mendeleyev Ridge and in the Makarov Basin (Table 4). The Canada Basin between 77 and 84°N had intermediate ages, while those at the southern edge of this basin were oldest (Table 4).

The slightly younger ages in the Makarov Basin compared to the Canada Basin are consistent with hypothesized circulation pathways for Atlantic-derived intermediate waters, which flow cyclonically through the Makarov and Canada Basins following bathymetric features such that waters in the southern Canada Basin have a longer flow path and have been removed from the atmosphere for a longer time compared to those along the Mendeleyev Ridge and in the Makarov Basin (e.g., Rudels et al., 1994; Schauer et al., 1997; Smethie Jr. et al., 2000). The oldest water in the southern Canada Basin is also located beneath the southern arm of the Beaufort Gyre, which accumulates surface water that has been recirculating around the Canada Basin; surface water ages based on the ingrowth of thorium-228 with its parent ^{228}Ra indicated that these waters have left the shelf at least 2.5 years ago, the longest of any of the surface waters sampled on the 2015 transect (Kipp et al., 2018). The ages of the UHL presented herein therefore show that the circulation pathways of the halocline mirror that of the underlying Atlantic layer. This suggests that halocline chemistry is likely modified via contributions from the Eurasian slopes, and that water originating on the Chukchi shelf loops around the Canada Basin rather than flowing directly into the southern basin (which would result in lower apparent ages).

Ventilation timescales between methods (SF_6, ^{3}H/^{3}He and ^{228}Ra/^{226}Ra) are generally consistent: all three tracers show an increase in halocline age from the Makarov Basin to the Northern Canada Basin to the Southern Canada Basin (Table 4; Figure 3). Although the ages for specific regions differ by up to 10 years across all three tracers, each individual tracer shows a similar geographic pattern and has significant differences in the age ranges for different regions. Radium ages skew slightly younger than the other two tracers; because Ra has a different source location (sediment rather than atmospheric), the offset likely indicates that there were inputs from the shelf sediments (which adds ^{228}Ra) after the water was out of contact with the atmosphere (which adds SF_6 and ^{3}H/^{3}He).

4. Biogeochemical Properties of the Upper Halocline

4.1. Macronutrients and Their Isotopes

The biogeochemical properties of the Amerasian Arctic Ocean, specifically those in the UHL, are distinct from other ocean basins. The subsurface nutricline in the Canada Basin features a prominent maximum in macronutrient (N, P, Si) concentrations associated with colder PWW, and a coincident maximum in apparent O_2 utilization (AOU) (Figure 2). The nutrient maximum originates from the inflow of nutrient-rich Pacific waters at Bering Strait and is enhanced by the near-bottom regeneration of organic matter from summer production on the Chukchi and East Siberian shelves (Granger et al., 2013; Jones & Anderson, 1986; Jones et al., 1998; Newton et al., 2013).

Mechanistically, the coincidence of the nutrient maxima and low dissolved O_2 concentrations in PWW likely arises from seasonal dynamics on the shelves (Figure 3, modified from Granger et al., 2018). Under ice cover in winter, the water column on the Chukchi shelf is isothermal and isohaline and is consequently well-mixed (Woodgate, Aagaard, & Weingartner, 2005). Given open leads in sea ice, dissolved O_2 in winter approach saturation (Nishino et al., 2016). In late spring, ice melt, river runoff, and increased solar radiation freshen and warm the surface, resulting in strong stratification that leads to the formation of PSW in the upper water column

Table 4
Categorization of Trace Metals and Their Isotopes Into Characteristic Distributions in the UHL

Theme 1: Diapycnal mixing dominated		Theme 2: Shelf influenced		Theme 3: Combination	
dGa	pP_L	dZn (+)	pFe_L pCo_L,	dBa (+)	pZn_L, pCu_L,
dCu	pP	dCd (+)	pMn_L, pV_L,	dNi (+)	pNi_L, pBa_L,
dU		dFe (+)	pTi_L, pAl_L,	dCo (+)	pCd_L, pCd, pNi,
$d^{230}Th$		$\delta^{114}Cd$ (−)	pMo_L, pCr_L,	dPb	pCu, pZn (+)
d^{231} Pa		$\delta^{56}Fe$ (−)	pMo, pFe, pMn,	dV (−)	
DOC		^{228}Ra	pV, pBa, pAl,	dMn (+)	
		^{226}Ra (+)	pCo, pCe, pPb		
		Hg (+)	(+)		

Note. Uncharacterized isotopes include ^{234}Th and ^{228}Th. (+) indicates an increase, (−) indicates a decrease relative to the PML and Atlantic water. No symbol indicates that it is hard to determine or varies between stations.

and isolation of PWW from the surface (Lowry et al., 2015; Pacini et al., 2019; Timmermans et al., 2014; Woodgate, Aagaard, & Weingartner, 2005). Seasonal phytoplankton blooms consume nutrients in PSW; sinking organic material is subsequently remineralized to inorganic nutrients in remnant PWW at the shelf bottom (Figure 3; Granger et al., 2018; Juranek et al., 2023; Lowry et al., 2015). Dissolved O_2 in remnant PWW is consumed in proportion to nutrients regenerated, resulting in high AOU in the remnant PWW that advects off-shelf during late summer and fall—at which time net poleward flows at Barrow and Herald Canyons are higher than in other seasons (Itoh et al., 2015; Pickart et al., 2005; Weingartner et al., 1998).

Despite the inflow of nutrient-rich Pacific waters to the Bering and Chukchi Seas (Arrigo & van Dijken, 2011; Hansell et al., 1993; Springer & McRoy, 1993), the Canada Basin downstream is oligotrophic (Tremblay et al., 2015). Once in the basin, the PWW nutrient reservoir is generally located below the euphotic zone and is suppressed from upwelling by stratification and limited vertical mixing (e.g., Jackson et al., 2010; Timmermans et al., 2008; Tremblay et al., 2014; Walsh et al., 2005). Recent increases in both Ekman convergence and freshwater input to the Canada Basin have increased stratification (Woodgate and Peralta-Ferriz, 2021; Yamamoto-Kawai et al., 2009), leading to a discernible deepening of the nutrient reservoir (McLaughlin & Carmack, 2010). Primary production in central Arctic surface waters is therefore largely recycled (Ji et al., 2019; Tremblay et al., 2015) and phytoplankton are subject to chronic nitrogen limitation, curtailing their biomass (Simpson et al., 2008; Taylor et al., 2013; Tremblay et al., 2015).

The influence of shelf processes on the biogeochemical properties of the UHL is further evident in the stable isotope ratios of nitrate and silicic acid. Measurements of the $\delta^{18}O\text{-}NO_3$ in the UHL covary with $\delta^{18}O\text{-}H_2O$, indicating that nitrate originated from nitrification (Granger et al., 2018)—the biological oxidation of ammonium from regenerated organic material—corroborating the notion that nitrate in the UHL originates from regeneration, which is likely advected from the shelves (Brown et al., 2016; Fripiat et al., 2018; Granger et al., 2011). The $\delta^{15}N\text{-}NO_3$, in turn, has a uniformly high value in the UHL (8‰) compared to the Atlantic water below (5‰) (Figure 2). The high $\delta^{15}N\text{-}NO_3$ value results in part from isotope fractionation due to benthic denitrification on the Bering and Chukchi shelves and is coincident with a substantial N-deficit ($N^* \cong -12$ μmol kg^{-1}, Figure 2 (Chang & Devol, 2009; Granger et al., 2011; Mordy et al., 2021; Zhuang et al., 2022). The high $\delta^{15}N\text{-}NO_3$ of the UHL distinguishes it from Atlantic-origin NO_3 throughout the Arctic Ocean basins and within the CAA and is a useful tracer of Pacific-origin waters (Lehmann et al., 2019, 2022).

The Si isotope ratios of silicic acid ($\delta^{30}Si\text{-}Si(OH)_4$) similarly track the Pacific-origin of dissolved silica (dSi) in the UHL. A subsurface minimum in $\delta^{30}Si\text{-}Si(OH)_4$ is associated with the subsurface dSi maximum in PWW (Figure 2), with values similar to those observed in BSI. The light UHL $\delta^{30}Si\text{-}Si(OH)_4$ signal is thought to derive from the relatively low value of subsurface $\delta^{30}Si\text{-}Si(OH)_4$ in the North Pacific (Reynolds et al., 2006) that is further modified by biological consumption in the Bering Sea, and benthic inputs derived from the dissolution of biogenic opal in shelf sediments (Brzezinski et al., 2021). Unlike nitrate, dSi persists into the PML, albeit decreasing toward the surface due to biological utilization. Values of $\delta^{30}Si\text{-}Si(OH)_4$ increase toward the surface due to characteristic assimilation isotope effects during biological uptake (Brzezinski et al., 2021; Giesbrecht & Varela, 2021; Liguori et al., 2021; Varela et al., 2016). Brzezinski et al. (2021) postulated that the elevated dSi in the PML may also derive from local riverine input, although the effect on $\delta^{30}Si\text{-}Si(OH)_4$ is not readily distinguishable due to the competing influence of fractionation from biological assimilation and the spatial and seasonal variability of the $\delta^{30}Si\text{-}Si(OH)_4$ values in Arctic rivers (Pokrovsky et al., 2013).

4.2. Inorganic and Organic Carbon

A dominant influence of shelf processes in the UHL is also evident in the distribution of dissolved inorganic carbon (DIC). A maximum in DIC and coincident minimum of pH_{sws} (pH on the seawater scale) are co-located with the AOU and nutrient maxima in UHL (Figure 2). These features are consistent with the remineralization of carbon photosynthetically produced on the shelf (Bauch et al., 2015; Brown et al., 2016; Ko & Quay, 2020).

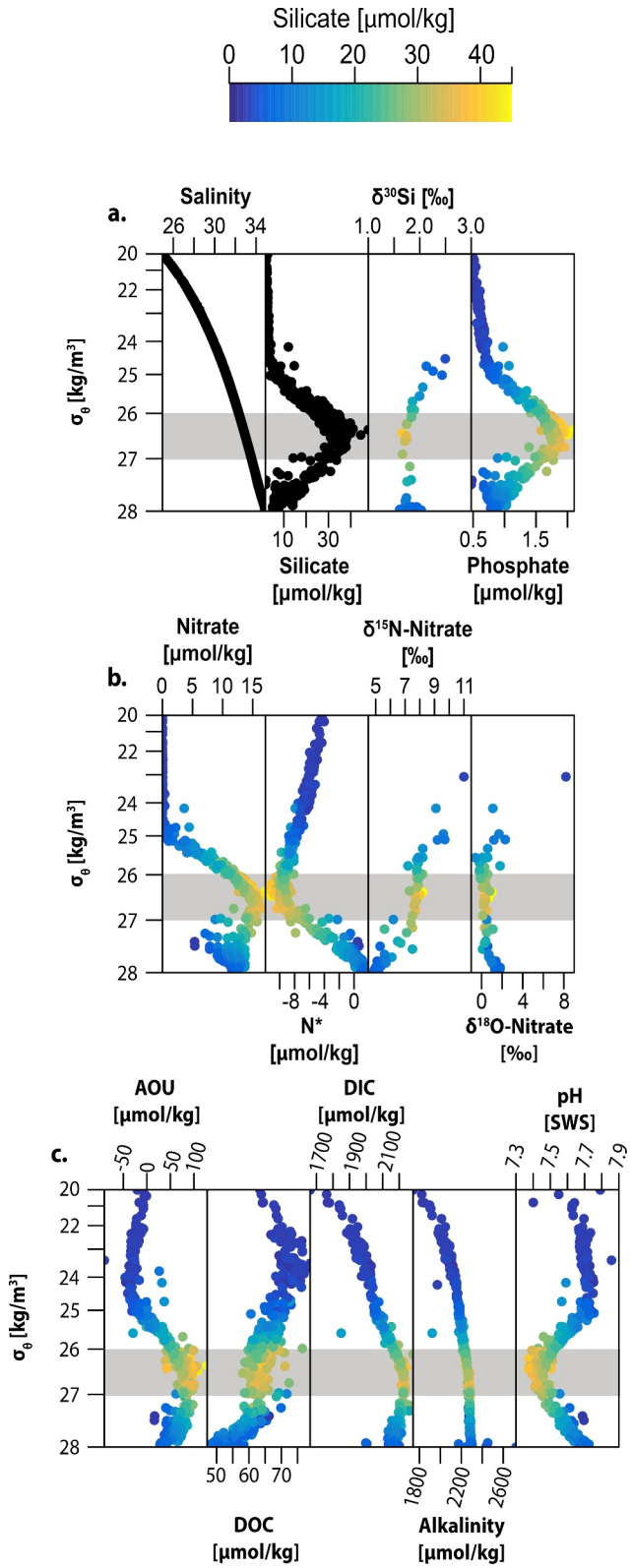

Figure 2. Biogeochemical properties of the UHL (gray shaded area) including (a) salinity, silicate, δ^{30}Si, phosphate, (b) nitrate, N*, δ^{15}N-nitrate, δ^{18}O-nitrate, (c) Apparent oxygen utilization (apparent O2 utilization), dissolved organic carbon, dissolved inorganic carbon, Alkalinity, and pH. The symbol color is silicate concentration, where high Si concentration indicates the core of the UHL.

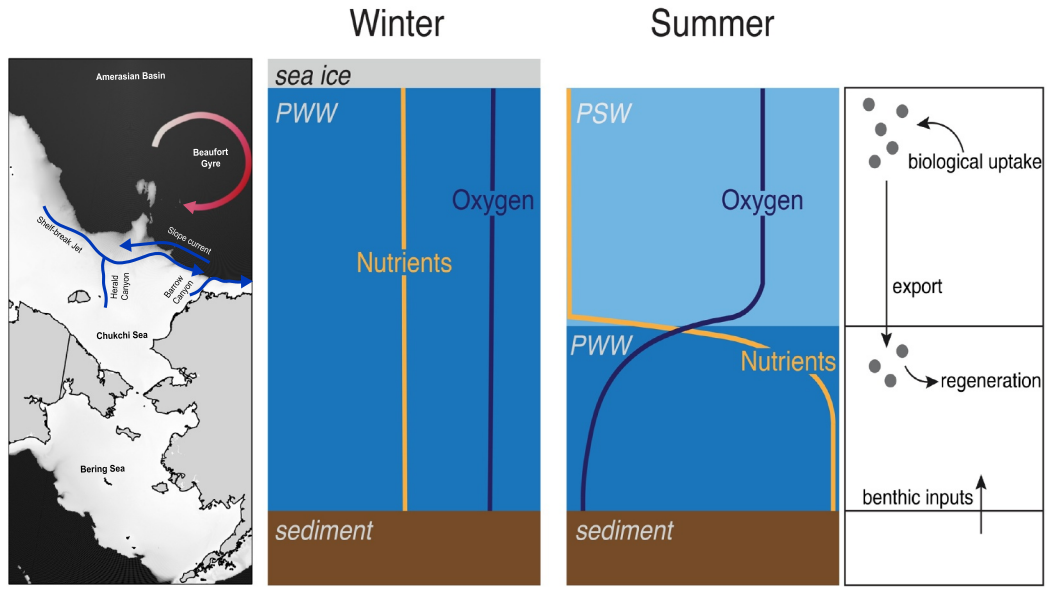

Figure 3. Seasonal dynamics of the Chukchi shelf. In winter, nutrients and dissolved oxygen are homogeneous in well-mixed newly formed Pacific Winter Water (PWW), and oxygen approaches saturation. In summer, nutrients are depleted at the surface in the relatively warm Pacific Summer Water and abundant at depth in the remnant PWW; the processes controlling this summer distribution are shown in the schematic on the right. Nutrients are consumed by primary producers at the surface and regenerated at depth following the export of organic material; benthic inputs can further enhance nutrient stocks. Nutrients sourced from water column and benthic regeneration are added to existing pools in remnant PWW. Oxygen is consumed proportionally. Modified from Granger et al., 2018. The leftmost panel indicates the general circulation of waters (blue arrows) as they are advected off the Chukchi Sea shelf and into the Amerasian Basin. The Beaufort Gyre circulation and qualitative age of halocline waters (see Section 3; white = younger, red = older) are depicted by the red gradient. Bathymetry is represented in greyscale from 0 m (white) to 500 m (black).

Barring some evidence of nonlinearity throughout the water column–especially in surface waters–due to the trace effect of respiration on alkalinity, the alkalinity distribution is predominantly driven by diapycnal mixing. There is no evidence of significant $CaCO_3$ dissolution in the UHL.

The surface of the Amerasian Basin provides a weak sink for anthropogenic CO_2 (Bates et al., 2006; Else et al., 2013; Ko & Quay, 2020; Woosley & Millero, 2020), thus anticipated decreases in alkalinity and pH_{sws} from continued freshening (H. Li & Fedorov, 2021) will render the Amerasian Basin an even weaker sink of anthropogenic CO_2.

Rivers contribute a significant amount of DOC to the surface Arctic regionally with the highest concentrations along GN01 measured in the river-dominated (i.e., Transpolar Drift) component of the PML (Figure 2), despite removal of DOC on Arctic shelves (Cooper et al., 2005; Hansell et al., 2004; Letscher et al., 2011). There is apparent endmember mixing between the riverine signal, BSI, and sea ice melt, with the latter diluting the DOC signal in the PML (Mathis et al., 2005). The DOC distribution from GN01 (Figure 2) generally agrees well with previous observations and interpretations (Amon et al., 2003; Mathis et al., 2005). High concentrations of dissolved organic matter, likely introduced by Eurasian rivers, have been found in UHL waters leaving the Arctic via the Fram Strait (Amon et al., 2003). Here, we report the highest individual DOC values (>70 μM) within the UHL, suggesting a shelf or river water source contributing to the Pacific-derived DOC signal.

4.3. Dissolved Gasses (N_2O, CH_4)

As with the nutrient tracers, biogenic gasses, and their isotopes in the UHL reflect the influence of shelf processes. Nitrous oxide (N_2O), a potent greenhouse gas produced during both nitrification and denitrification, has a prominent maximum in PWW that is ~30% above atmospheric saturation (Figure 4a), in contrast to near atmospheric equilibrium at the surface. The N_2O maximum persists basin wide, as there is no sink of N_2O in

10.1029/2024GB008342

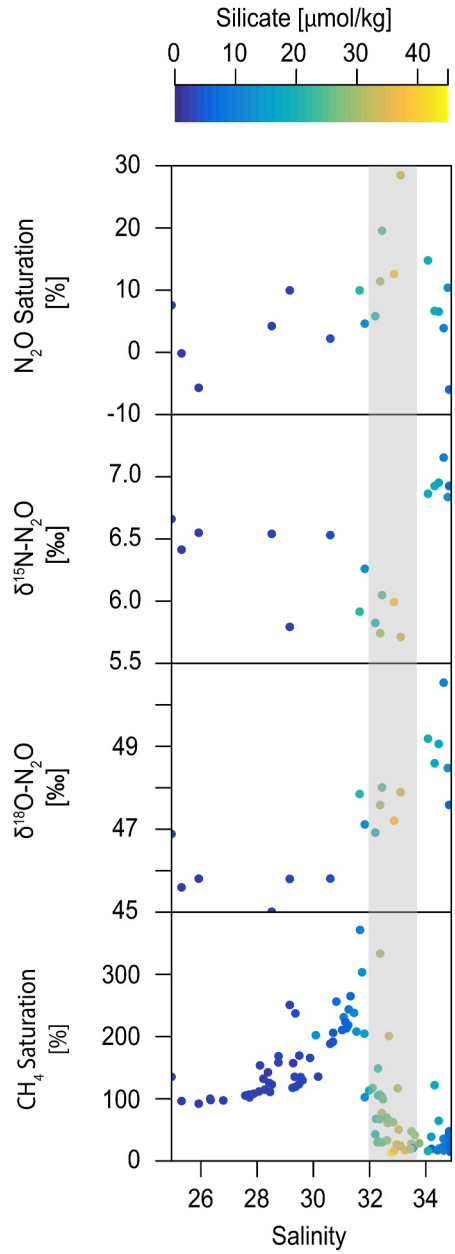

Figure 4. Dissolved gasses. From top to bottom: N_2O saturation (%), $\delta^{15}N$-N_2O (‰), $\delta^{18}O$-N_2O (‰), and CH_4 saturation (%) off the shelf (>73°N, <84°N) and within the upper 1,000 m. Symbol color is silicate concentration to denote UHL.

oxygenated waters. This feature has been observed previously in this region (Fenwick et al., 2017; Hirota et al., 2009). The N and O isotopic ratios of N_2O ($\delta^{15}N$-N_2O and $\delta^{18}O$-N_2O) reported here and by others (Toyoda et al., 2021) reveal end-member mixing of atmospheric and marine biogenic N_2O. A minimum in bulk $\delta^{15}N$-N_2O (5–6‰) and high $\delta^{18}O$-N_2O (47–48‰) in PWW together suggest that the biogenic N_2O is a product of nitrification and that it is partially consumed by denitrification in shelf sediments. A dominant sediment source of N_2O is further revealed by depth profiles on the Chukchi shelf, where N_2O concentrations are generally highest at the bottom (Fenwick et al., 2017; Toyoda et al., 2021). The N_2O bottom water maximum corresponds to the prominent N deficit (N* minimum) noted above. Nevertheless, in spite of exhibiting a large shelf area rendering the system propitious to benthic denitrification (Chang & Devol, 2009), the Amerasian Basin is considered a minor source of N_2O to the atmosphere (Fenwick et al., 2017).

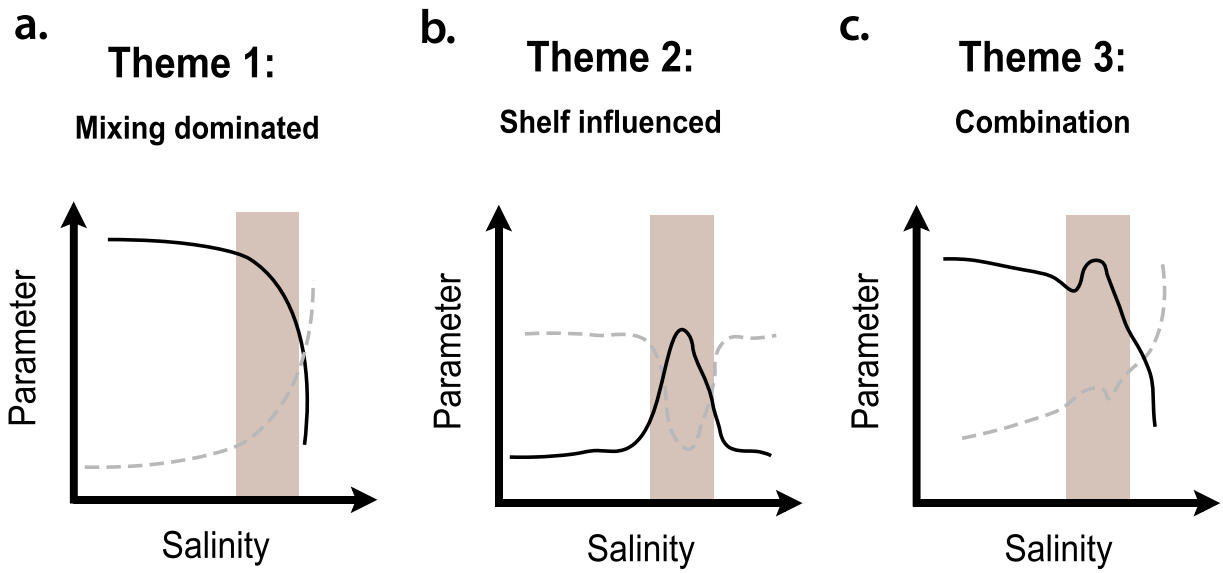

Figure 5. The element-salinity relationship can be characterized in 3 general themes: (a) diapycnal mixing dominated, (b) shelf influenced, (c) a combination of mixing and shelf influence. The gray dashed line indicates that some elements have opposing patterns (i.e., higher concentrations in the fresh Polar Mixed Layer vs. lower concentrations in the saltier Atlantic layer). The salinity range for the UHL is shaded (tan) on each panel. Note that this paradigm does not preclude other processes affecting trace elements and isotopes (TEIs) in the UHL including biotic and abiotic scavenging.

Methane (CH_4), which is generally short-lived in oxygenated water, has a maximum in PWW that is contiguous with the Chukchi shelf but is not conserved basin-wide (Y. Li et al., 2017), likely due to microbial oxidation. Methane on the shelf and slope region may derive from a variety of sources but can be coarsely divided into biogenic and geologic, i.e., from active microbial degradation of organic material and from seepage of fossil methane. On the shelf, CH_4 is highest at the sediment interface as a result of biogenic methane production, which was determined by isotopic analysis (Kudo et al., 2022). Methane data from the 2015 GEOTRACES cruise indicate a maximum in saturation at salinity of 30–32 (likely PSW) that is not coincident with the UHL (PWW) silicate maximum. The highest CH_4 saturations were observed in bottom waters at the shelf break and on the shelf (Whitmore & Shiller, 2016), which is consistent with a benthic source of CH_4 and rapid oxidation and dilution in the water column (Manning et al., 2022). In the Amerasian Basin, CH_4 has a near surface (<100 m) maximum (Figure S1 in Supporting Information S1) co-located with the chlorophyll maximum, a widely observed feature in other ocean basins (N. J. P. Owens et al., 1991). This result from 2015 is consistent with previous observations in the Amerasian Arctic (e.g., Kitidis et al., 2010). When sea ice is present, there is a capping effect of the ice which could lead to this maximum (Kitidis et al., 2010) and substantially influences the flux of methane from the surface ocean to the atmosphere (He et al., 2013; Lorenson et al., 2016). Thus, the CH_4 maximum appears to be associated with local surface water processes, rather than from distal advected sources, and hence is not a suitable tracer over broad spatial ranges.

5. Trace Element and Isotope Distributions in the Upper Halocline

Origins and transformations of the UHL become apparent when TEIs are plotted against salinity. Using this framework, we classify tracers in three distinct themes that illustrate the dominant processes shaping the chemical and isotopic distributions of each tracer in the open basins: (Theme 1) diapycnal mixing dominated, (Theme 2) shelf-influenced, or (Theme 3) a combination of the preceding two processes (Figure 5). Importantly, we establish this framework to help group the predominant processes controlling element distributions in the UHL but note that there are likely multiple influences on individual element profiles. For example, many elements show evidence of particle scavenging in the UHL that may not be immediately apparent from their profiles, but will be discussed further in Section 6.

Away from the shelf, TEIs typically conform, if sometimes imperfectly, to these three themes. Theme 1 tracers exhibit mixing between endmembers: surface (fresher), Pacific-origin waters, and deep (saltier, Atlantic-origin) water. A shelf source or sink is not required to explain their distribution. This results in linear or curvilinear

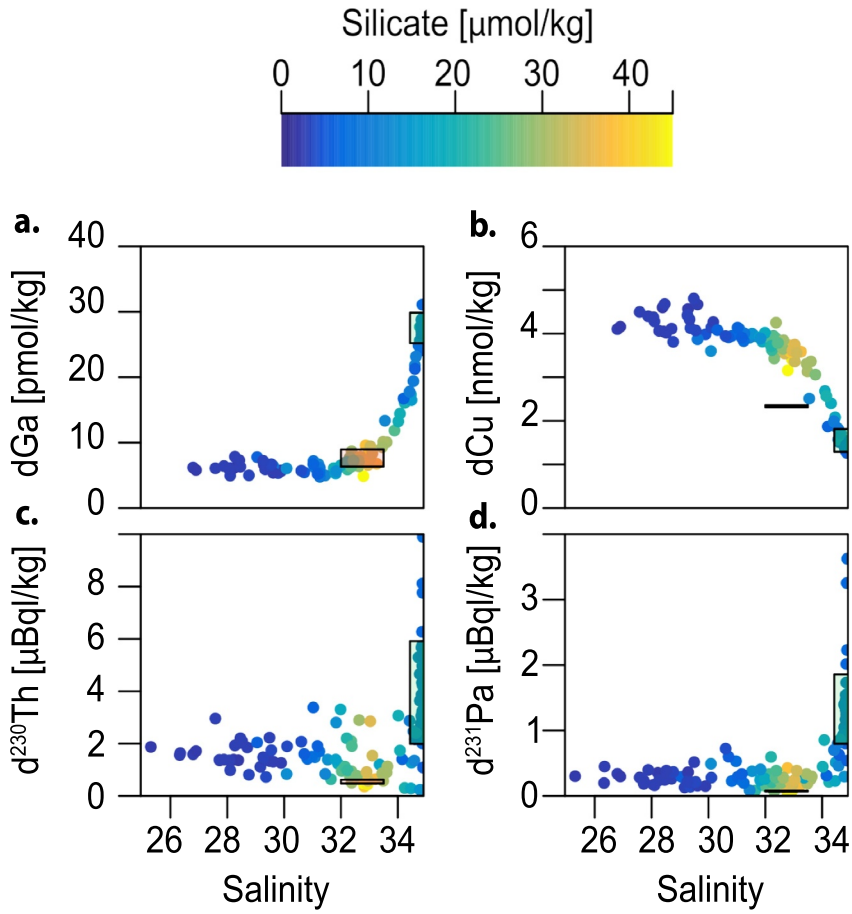

Figure 6. Theme 1 TEIs versus. salinity: Mixing-dominated. (a) dissolved Cu (nmol/kg), (b) dGa (pmol/kg), (c) $d^{230}Th$ (µBq/kg), (d) d^{231} Pa (µBq/kg). The symbol color is silicate concentration to denote the bounds of the UHL. Red rectangles are used to indicate the Bering Sea Inflow concentration/salinity range for each element as defined in Section 4. Where the concentration range of Bering Sea Inflow is very small, the box may appear as a bold line. Green rectangles indicate the Atlantic Water endmember as an average plus or minus one standard deviation. Since the salinity range of Atlantic Water is very small, the range of the salinity used for drawing the box has been inflated by 10% relative to observations of the Atlantic Water endmember.

distributions of elements (Section 5.1). Theme 2 parameters are relatively uniform in the surface and deep waters of the basins, and have a source (or sink, gray dashed line, Figure 5) over the shelves. Like Theme 1, Theme 3 tracers also exhibit mixing between multiple endmembers, but are also influenced by modifications on the shelf. Further, the placement of elements within these categories is with consideration to the "Pacific" endmember, which we define as the concentration observed in the BSI, estimated by averaging above and below the mixed layer depth at stations 4 and 5 (red box in Figures 6, 7 and 9). We also include Atlantic Water endmembers in the subsequent figures for reference (green box in Figures 6, 7 and 9), which are determined as the average value of data between sigma theta isopycnals (27.87–28.02 kg m^{-3}) associated with Fram Strait Branch Water and Barents Sea Branch Water (e.g., Dmitrenko et al., 2015; Rudels et al., 1994, 2000; Schauer et al., 2002; Shimada et al., 2004). Although they make an important contribution to the upper Arctic Ocean, we do not estimate river endmembers for most of these elements as there is insufficient data for the majority of these parameters; river endmembers also tend to be variable by drainage basin.

5.1. Theme 1: Diapycnal Mixing Dominated Dissolved TEIs

Tracers can be broadly categorized as conservative (concentrations change solely by mixing) or non-conservative (those that are influenced by biological or chemical processes in addition to mixing). At best, geochemical tracers in the UHL are "quasi-conservative" where the chemical or biological processes that influence the element are

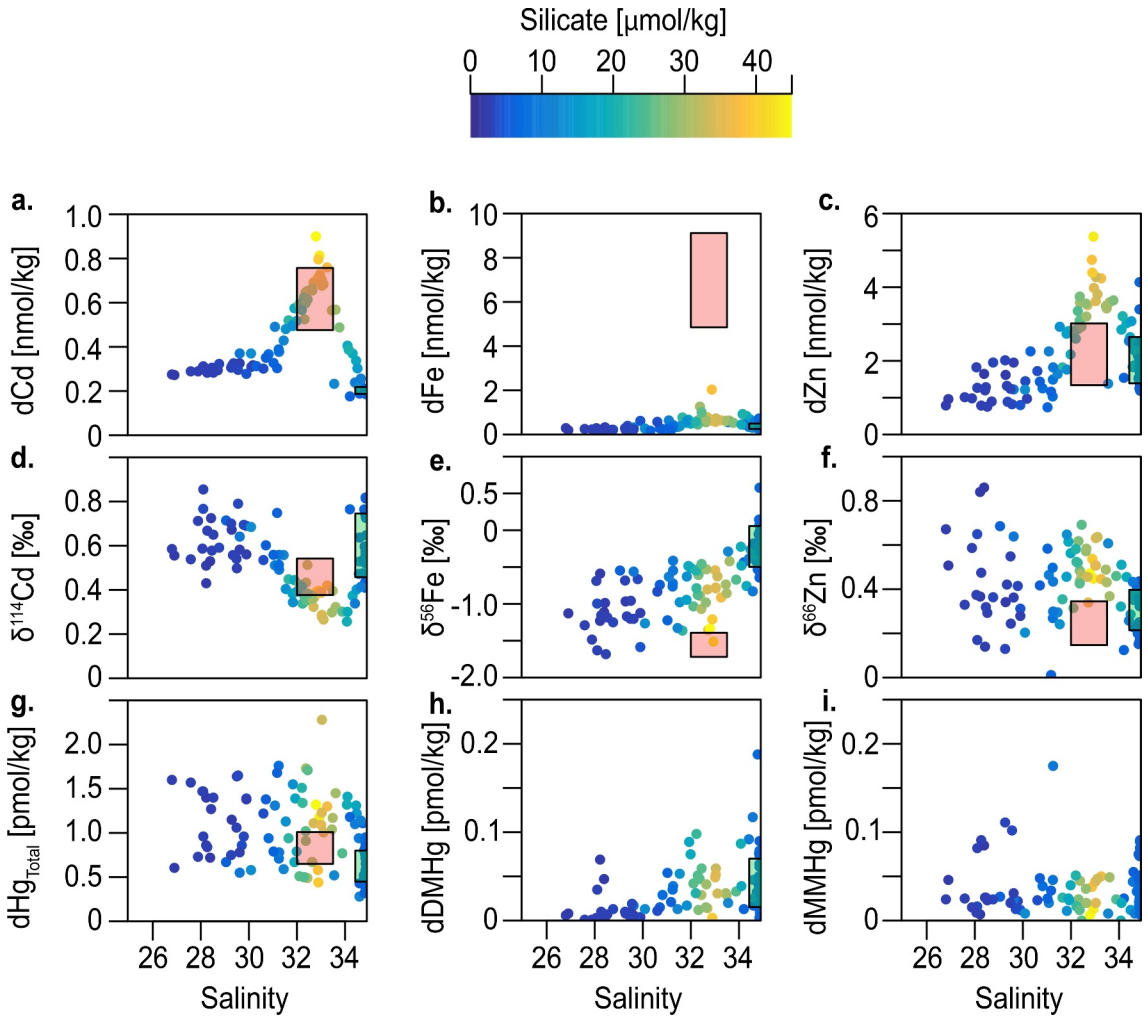

Figure 7. Theme 2 TEIs versus. salinity: shelf influenced. (a) dCd (nmol/kg), (b) dFe (nmol/kg), (c) dZn (nmol/kg), (d) δ^{114}Cd (‰), (e) δ^{56}Fe (‰), (f) δ^{66}Zn (‰), (g) dHgT (pmol/kg), (h) dDMHg (pmol/kg), (i) dMMHg (pmol/kg). The symbol color is silicate concentration to denote the bounds of the UHL. Red boxes are the Bering Sea Inflow range for each element. Green rectangles indicate the Atlantic Water endmember as an average plus or minus one standard deviation. Since the salinity range of Atlantic Water is very small, the *x*-axis bounds have been expanded by 10%. Note that dDMHg and dMMHg data are missing at stations used in the endmember calculations.

minimal relative to the element's observed concentrations. The element-salinity relationships for the distributions of these elements tend to be curvilinear: in part because of multiple water masses and their relative endmembers, but non-linearity between endmembers may be because diapycnal mixing is suppressed within the halocline and thus vertical mixing rates differ throughout the halocline. Curvilinear distributions are concave or convex depending on whether elemental concentrations are high or low in the PML. This distribution results from diapycnal mixing between the river and ice melt-influenced PML (Figure 5a) and the underlying Pacific-derived UHL (S ~32.5). At higher salinity (S >32.5), Pacific-derived waters mix with the Atlantic layer (saltier, far right) (Figure 5a).

Dissolved Ga and Cu distributions are both driven by the mixing of low salinity surface waters with higher salinity Pacific and Atlantic waters (Figure 6). Globally, Cu is typically sourced from river water input and atmospheric deposition (Jacquot & Moffett, 2015; Richon & Tagliabue, 2019) but is low in the surface ocean away from the continents due to biological uptake (Bruland et al., 2014). Contrary to other ocean basins, dCu in the Arctic Ocean is high in the surface and declines with depth, in the UHL and AW (Figure 6). The high surface concentrations reflect high river water input (Charette et al., 2020; Jensen et al., 2022) and a large freshwater reservoir (Serreze et al., 2006). The BSI endmember of dCu is low relative to the observed UHL waters (Figure 6); we expect that this may be driven by a misrepresentation of the BSI endmember with potentially high seasonal variability in dCu

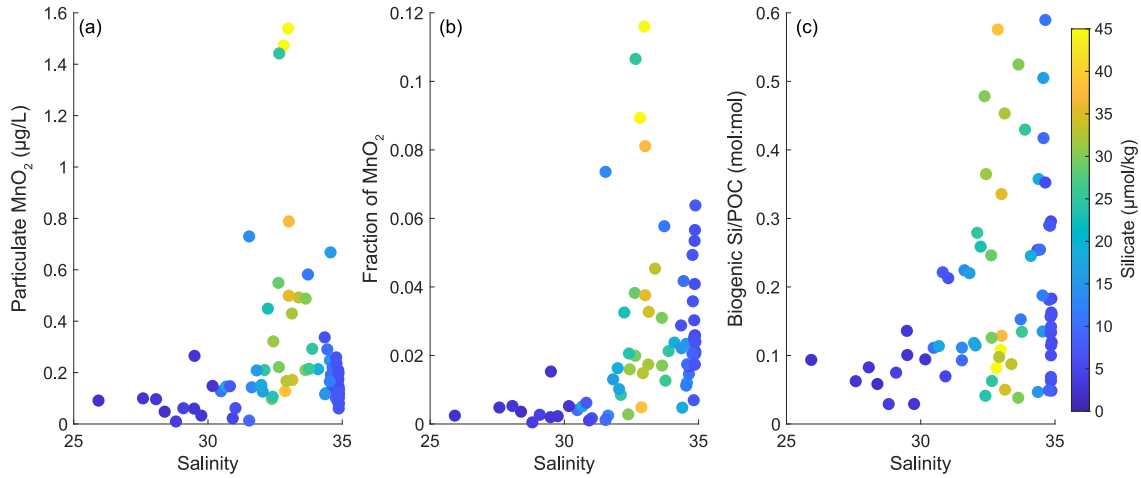

Figure 8. Particle composition (particle size ≥0.8 µm) versus salinity within the UHL. (a) Concentrations of manganese oxide (MnO_2) (µg/L); (b) the fraction of MnO_2; (c) the molar ratio between biogenic silica and particulate organic carbon (mol:mol). The symbol color is silicate concentration to denote the core of the UHL.

driven by Yukon (and other river) discharge and seasonal biogeochemical cycling. The salinity-dCu does not indicate strong removal on the Chukchi shelf or in the basin, likely due to the large riverine contribution overshadowing any depletion due to biological uptake (Cid et al., 2012; Jensen et al., 2022). Conversely, dGa is elevated in Atlantic waters and low in Pacific and freshwater, a characteristic driven by differences in the supply of atmospheric dust to the North Atlantic Ocean (relatively high) and North Pacific Ocean (relatively low;

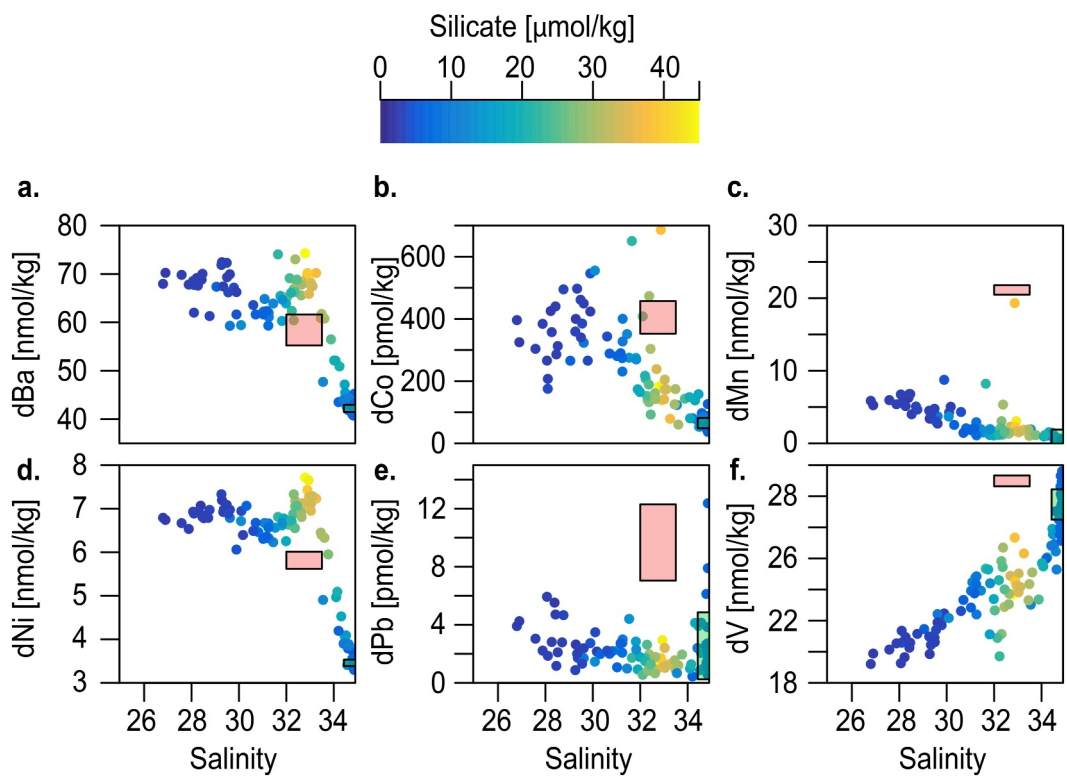

Figure 9. Theme 3 TEIs versus. salinity: Combination. (a) dBa (nmol/kg), (b) dCo (pmol/kg), (c) dMn (nmol/kg), (d) dNi (nmol/kg), (e) dPb (pmol/kg), (f) dV (nmol/kg). The symbol color is silicate concentration to denote the bounds of the UHL. Red boxes are the Bering Sea Inflow range for each element. Green rectangles indicate the Atlantic Water endmember as an average plus or minus one standard deviation. Since the salinity range of Atlantic Water is very small, the *x*-axis bounds have been expanded by 10%.

McAlister & Orians, 2015; Orians & Bruland, 1988; Shiller & Bairamadgi, 2006; Whitmore et al., 2020). Although dGa has an atmospheric source, dust deposition in the Arctic Ocean basins is often low due to retention of dust in sea ice cover (rather than directly deposited to the ocean surface) and atmospherically derived dGa does not appear to be a substantial source to the PML (Marsay et al., 2018; Whitmore et al., 2020). Despite being somewhat prone to scavenging in particle-rich settings, distributions of dGa in the Arctic Ocean basins appear conservative along isopycnals (Whitmore et al., 2020). Thus, it may be leveraged as a tracer of mixing between Pacific and Atlantic waters across the Arctic with little evidence of external sources and sinks (Whitmore et al., 2020).

^{230}Th ($t_{½} \sim 75.4$ kyr) and ^{231}Pa ($t_{½} \sim 32.7$ kyr) have distributions similar to those of dGa (Figure 6). Activities of longer-lived ($t_{½} > 10$ kyr) dissolved radioisotopes have been widely used in the Arctic Ocean and in other basins to investigate circulation and particle dynamics (Bacon & Anderson, 1982; Gdaniec et al., 2020; Hayes et al., 2018; Hoffmann et al., 2013; Lerner et al., 2017; Pavia et al., 2019). The source of these isotopes is the decay of parent isotopes naturally present in seawater. ^{231}Pa and ^{230}Th have uranium parents, which behave conservatively in marine environments and are correlated with salinity (S. A. Owens et al., 2011). Even with brine formation and significant freshwater inputs in the Arctic, a linear uranium-salinity relationship consistent with other oceanic regions is observed (Not et al., 2012). Unlike their conservative parents, ^{231}Pa and ^{230}Th are particle reactive; ^{230}Th has a high particle affinity and an oceanic residence time of decades, while ^{231} Pa is slightly more soluble and has a residence time of centuries. The strong mixing pattern observed in the ^{230}Th and ^{231}Pa activities (Figure 6) is likely related to the long half-lives and oceanic residence times of these isotopes compared to the residence time of the water in the halocline (~6–23 years, see Section 3). The short-lived dissolved ^{234}Th ($t_{½} \sim 24$ days) behaves dissimilarly to ^{230}Th and ^{231}Pa and increases slightly with increasing salinity but does not match the Theme 1 patterns.

5.2. Theme 2: Shelf-Influenced TEIs

Element-salinity distributions that have a distinct peak or trough within the salinity range for the UHL indicate shelf processing during the origin and formation of the halocline itself. A peak is observed in the UHL for all macronutrients, N_2O gas, and many dissolved and particulate trace metals. Thus, the UHL becomes the major source or reservoir for these elements in the Canada Basin.

Many bioactive trace metal profiles in the ocean are heavily influenced by biological uptake and regeneration, thus sharing similar distributions to the macronutrients. In the Amerasian Basin, uptake and regeneration signals are primarily formed on the shelves. Advection of shelf waters into the basin results in distinctive profiles in the open basins, where some of the bioactive dissolved trace metals exhibit a subsurface peak coinciding with the nutrient maximum. Elements such as dFe, dZn, dCd (Figure 7a–7c), as well as the major macronutrients (Figure 2), fit into Theme 2. These elements have a maximum concentration in the salinity range of PSW and PWW (S ~31–33.1). On the Chukchi shelf, dFe, dZn, and dCd appear to share a benthic maximum with Si. For dFe and dZn, maxima in PWW result from diagenetic release of Fe from the sediments (Jensen, Morton, et al., 2020) and the release of Zn from Si-rich organic matter (Jensen et al., 2019), respectively. Although dCd has UHL maximum that is a similar concentration as the BSI, it is likely still heavily modified by shelf biogeochemical cycling and sedimentary exchange processes. Specifically, dCd has strong correlation with tracers of sedimentary remineralization and enrichment compared to P in shelf bottom waters (Zhang et al., 2019).

Metal isotope ratios (Figures 7d–7f) corroborate the influence of both remineralization and reductive dissolution in shelf bottom waters on the basin distributions of advected dissolved metals. Low δ^{56}Fe values, which are indicative of reductive dissolution, were observed along the Chukchi shelf and this signal persists into the UHL (Zhang et al., 2021), leading to a trough in the δ^{56}Fe-salinity plot (Figure 7e). δ^{114}Cd is also depleted in shelf bottom waters and within the halocline relative to the PML and AW (Figure 7d), indicative of Pacific-origin or remineralization-influenced waters, both of which skew to relatively low isotope ratios due to organic matter decomposition (Zhang et al., 2019). Values of δ^{66}Zn (Figure 7f) align more closely with Theme 3 (Section 5.3) but are nevertheless consistent with the release of dZn in shelf sediments that persists within the UHL.

Mercury concentrations and speciation are influenced by shelf interactions, although correlations with salinity are impacted by gaseous mercury species and sea ice dynamics that control air-sea exchange (Figures 7g–7i). Elemental Hg (Hg^0) is typically sourced by atmospheric deposition, rivers, soil runoff, and groundwater (Dastoor et al., 2022; Mason et al., 2012). It accumulates in the Arctic PML when sea ice cover limits evasion to the

atmosphere (Agather et al., 2019; Bowman et al., 2020). Total dissolved Hg (dHg) can be mobilized from sediments where microbial production of the neurotoxin monomethylmercury (MMHg) and subsequent formation of dimethylmercury (DMHg) may occur (Agather et al., 2019; Mason et al., 2012). While concentrations of dHg are lower in the Arctic compared to other global oceans, MMHg and DMHg were elevated over the Chukchi shelf and DMHg in particular had a peak in the halocline (Agather et al., 2019), suggesting high concentrations over the shelf persist in the halocline. Thawing permafrost and sea ice are significant reservoirs of Hg in the Arctic, potentially contributing to enhanced MMHg and DMHg production leading to cascading ecosystem effects as the Arctic warms (Dastoor et al., 2022).

The Amerasian Basin has a distinct particle maximum associated with Pacific-origin halocline waters against an otherwise very low particle abundance in the oligotrophic central Arctic Ocean (Xiang et al., 2022; Xiang & Lam, 2020). Labile (_L) particulate trace metals (>0.45 μm) such as pMn_L, pCo_L, pV_L, pAl_L, and pFe_L were noticeably elevated on the Chukchi shelf and within the UHL (Twining et al., 2019), following a Theme 2 distribution (Figure S2 in Supporting Information S1, Table 3). Chemical signatures of particle composition in the UHL, including concentrations and relative fractions of MnO_2, and biogenic Si to particulate organic carbon (POC) ratios (Figure 8), suggest the importance of lateral transport from the Chukchi shelf and potentially other nearby shelves into the central Arctic Ocean (Xiang & Lam, 2020). Concentrations of MnO_2 are more elevated within the UHL than Fe oxyhydroxides. This difference is due to slower oxidation kinetics of dMn(II) compared to dFe(II) released from shelf sediments during sediment diagenesis allowing dMn to be transported a longer distance into the central basin before it is oxidized (Jensen, Morton, et al., 2020; Vieira et al., 2019; Xiang & Lam, 2020).

5.3. Theme 3: Combination—Mixing and Shelf Influenced TEIs

Many elements are also significantly influenced by both diapycnal mixing and shelf modification. These elements appeared to be mixed between surface and Atlantic waters (Theme 1) but also displayed noticeable peaks or troughs within the UHL salinity range (Theme 2). Two prevailing profile types emerged: one with high concentrations in surface waters, possibly correlated to freshwater/riverine input, displaying a peak in the halocline, and declining to Atlantic concentrations (Figure 5c). Alternatively, concentrations may be low on the surface with a peak in the halocline and continue to increase to Atlantic concentrations (gray dashed line, Figure 5c).

Trace elements that fall into this category can be bioactive/"nutrient-type" (e.g., dNi, dBa) or scavenging prone (e.g., dPb, dV, dMn) or hybrid-type (dCo). As noted in Section 5.2, element profiles in the Arctic Ocean are atypical compared to global distributions. Typically, dNi is low in surface waters and increases with depth, following the distribution of both Si and P (Middag et al., 2020). Barium is also correlated with Si (Wolgemuth & Broecker, 1970), but unlike the bioactive trace metals there is no known Ba requirement for enzymes in phytoplankton (Horner et al., 2021). Both dNi and dBa have elevated concentrations in Arctic rivers relative to seawater (Cooper et al., 2008; Guay & Falkner, 1997), leading to pervasively high concentrations in the PML (Figures 9a and 9d). The presence of a peak in dNi and dBa in the UHL suggests a non-negligible source from shelf sediments, as well as the influence of river runoff incorporated into the UHL (Jensen et al., 2022; Whitmore et al., 2022).

Dissolved Mn is also sourced from both rivers and shelf sediments in the Arctic Ocean (Colombo et al., 2020; Jensen, Morton, et al., 2020), leading to high concentrations in shelf bottom waters, the PML, and the UHL. Abundant freshwater sources lead to high dMn at low salinities in the Amerasian Basin (Figure 9c) and lack of removal processes and potential photoreduction helps to maintain the high dMn in the PML (Gerringa et al., 2021; Jensen, Morton, et al., 2020; Xiang et al., 2021). A local peak in dMn in the UHL (Figure 9c) implies supply of dMn from shelf bottom waters (Jensen, Morton, et al., 2020). Away from the shelves, dMn concentrations in the UHL are rapidly attenuated due to scavenging and oxidation, as seen for dFe and dPb (Colombo et al., 2019; Jensen, Morton, et al., 2020). Oxidized Mn in the UHL potentially drives scavenging of other TEIs (Section 5).

The dCo is elevated over the Chukchi shelf relative to Pacific water, and this signature is preserved in the Amerasian Basin PML. However, dCo displays a minimum in the underlying halocline, which is associated with scavenging (scavenging is discussed further in Section 6; Bundy et al., 2020). This is unique to the Amerasian Basins, and contrasts with the "nutrient-type" or "hybrid-type" depth distribution observed in other (non-Arctic) ocean basins (Chmiel et al., 2022; Saito et al., 2017). The dCo is heavily influenced by shelf processes, effectively masking any biological uptake signal. Similar to dCo, dV, which is globally low in surface waters and increases with depth (Ho et al., 2018), is depleted within the UHL relative to the BSI (Figure 9f). Unlike dCo, dV is also low in the PML, indicating the influence of riverine and sea ice melt endmembers. The high concentrations of MnO_2

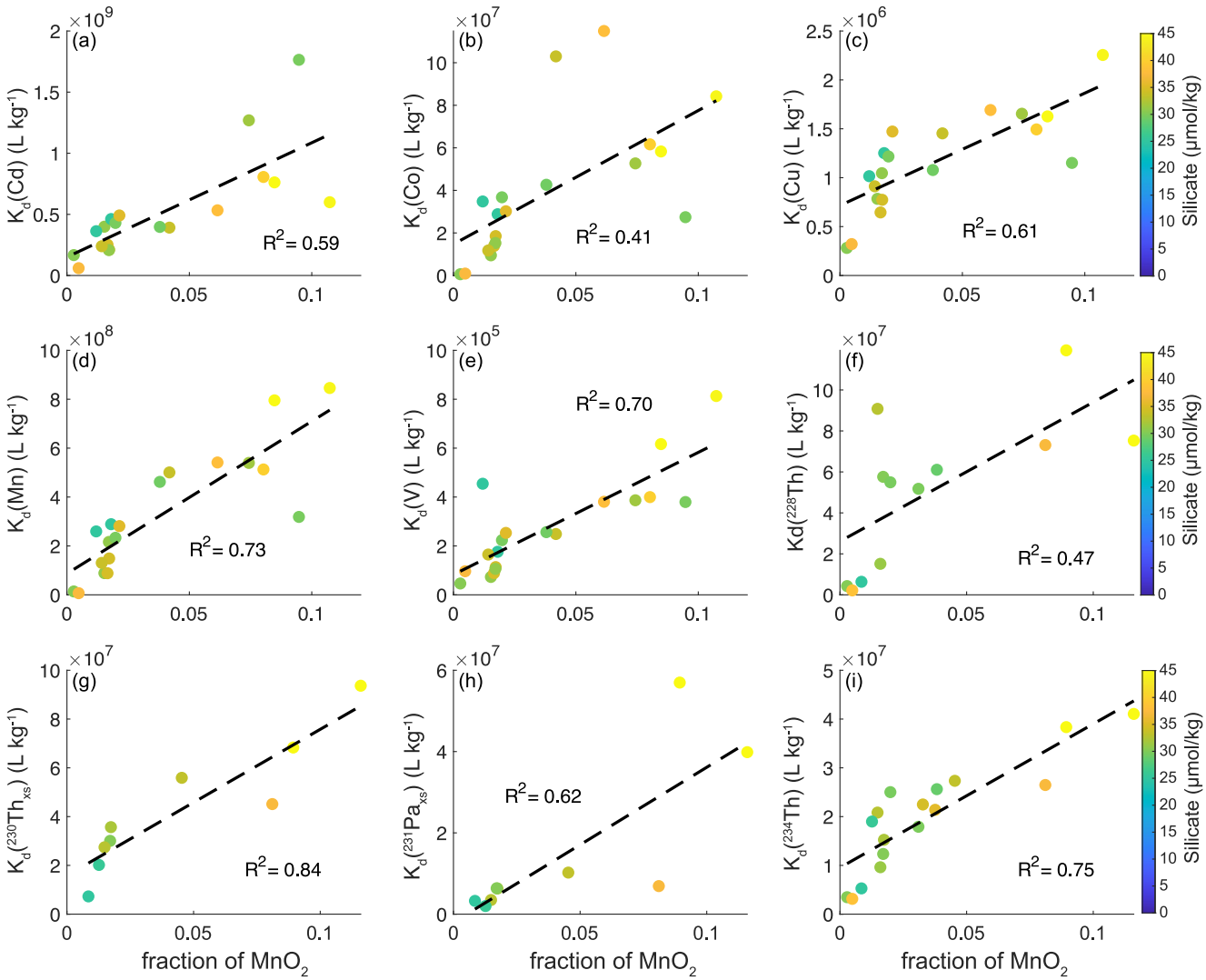

Figure 10. The relationship between the partitioning coefficient K_d of different TEIs and the fraction of manganese oxides within the core of UHL (where silicate concentrations are ≥25 µmol/kg). (a) Cd; (b) Co; (c) Cu; (d) Mn; (e) V; (f) ^{228}Th; (g): excess ^{230}Th; (h) excess ^{231} Pa; (i) ^{234}Th. The dashed lines are linear regression fits ($p < 0.05$) and the color bar is silicate concentrations. The coefficient of determination of each fit is displayed in the subplot. Additional parameters are shown in Figure S3 in Supporting Information S1.

in the UHL (Xiang & Lam, 2020) contribute to scavenging of dCo and dV within the halocline (Whitmore et al., 2019; see Section 6). However, the scavenging of these metals by MnO_2 is likely also biologically related, and the diminished scavenging in surface waters may be due to the lower abundance of MnO_2.

Dissolved Pb was elevated on the Chukchi shelf but did not have a discernible peak or trough within the UHL. In fact, dPb did not fit cleanly into any of the three themes as it is similarly elevated in the PML, PSW, and underlying Atlantic waters, and displays a small peak in the UHL at some stations (Figure 9e). The global distribution of Pb in the ocean is heavily influenced by anthropogenic contamination of Pb to the surface ocean (Boyle et al., 2014). While aerosol deposition of Pb is markedly less than in the dust-influenced North Atlantic by roughly an order of magnitude, anthropogenic pollutants from the surrounding continents lead to significant Pb in Arctic aerosols, potentially contributing to elevated concentrations in the PML found in this study. Freshwater sources such as sea ice melt and North American/Eurasian rivers may be another source of PML in the Canada Basin (Colombo et al., 2019; Newton et al., 2008). Elevated in both the North Pacific and North Atlantic, high dPb concentrations entering through the Bering Strait and dPb mobilized during remineralization on the Chukchi shelf are likely attenuated due to scavenging by particulates along the shelf break (Colombo et al., 2019; Nozaki

et al., 1997), similar to dMn and dFe. The peak in dPb above the UHL has been previously observed in the Canada Basin and is traceable through the CAA (Colombo et al., 2019).

Some bottle particulate species were elevated in the UHL and also in the PML and/or overlying PSW. Unlike the Theme 2 particulate species above, many did not follow their corresponding dissolved species theme categorizations. For instance, while dZn, dCd, and dCu fell into Themes 1 and 2, pZn_L, pZn, pCd_L, pCd, and pCu_L, pCu all show Theme 3 patterns off-shelf (Figure S1 in Supporting Information S1, Table 3). Additionally, pNi_L, pNi, and pBa_L were all elevated in both surface and UHL waters, much like dNi and dBa. Enrichment of these TEIs in the UHL likely results from lateral advection of authigenic or biogenic particles formed over the shelf (Whitmore et al., 2022), consistent with high biogenic silica to POC ratios as a result of lateral transport of shelf-derived particles (Xiang & Lam, 2020).

6. Particle Cycling of Trace Elements in the Halocline

Concentrations of MnO_2 within the UHL are notably high, reaching up to one order of magnitude higher than those found near vents of the East Pacific Rise (Lam et al., 2018; Xiang & Lam, 2020). Since MnO_2 are known as the "scavenger of the sea" (Goldberg, 1954), many TEIs in the UHL are likely substantially influenced by Mn oxide scavenging. We calculated for all TEIs the bulk partition coefficient K_d, an index for scavenging affinity (Bam et al., 2020; Cui et al., 2021; Hayes et al., 2015; Pavia et al., 2018). The K_d (unit: L/kg) for an element (E) is defined as

$$K_d(E) = \frac{pE_{excess}}{dE \times SPM},$$

where pE_{excess} and dE are non-lithogenic (excess) particulate and dissolved concentrations, respectively, and (suspended particulate matter) SPM is the concentration of suspended particulate matter.

Most TEIs have a significant positive correlation between K_d and the compositional fraction of MnO_2 (f_{MnO_2}; calculated as $[MnO_2]/[SPM]$) in total particles (≥1 μm) within the UHL (Figure 10 and Figure S3). Dissolved Mn and V are prone to strong scavenging by MnO_2 ($R^2 \geq 0.7$; $p \ll 0.01$). Likewise, scavenging of dCu, dCd, and dCo by MnO_2 is potentially an important removal process ($R^2 > 0.4$; $p < 0.01$). Particulate Co and V have a pronounced increase of similar magnitudes within the UHL (Figure S1 in Supporting Information S1). A better correlation between K_d and f_{MnO_2} exists in V ($K_d(V) = 5.0 \times 10^6 \times f_{MnO_2} + 8.3 \times 10^4$; $R^2 = 0.70$) than Co ($K_d(Co) = 6.3 \times 10^8 \times f_{MnO_2} + 1.5 \times 10^7$; $R^2 = 0.41$), possibly pointing to a stronger affinity of V to MnO_2 than Co. All four scavenging-prone Th and Pa isotopes' K_d values correlate well with f_{MnO_2} (R^2 from 0.47 to 0.84, $p < 0.05$; Figure 10). These high R^2 values indicate similar levels of correlation with f_{MnO_2} to those seen with Mn and V, reflecting the strong influence of MnO_2 on Th and Pa scavenging and distributions in the UHL (Hayes et al., 2015; Lee et al., 2021; Pavia et al., 2018).

Fe, Ni, and Pb have insignificant relationships between K_d and f_{MnO_2} ($p > 0.05$; Figure S3 in Supporting Information S1). The lack of a significant relationship for Ni suggests that scavenging removal is minor during the transport of dNi within the UHL (Jensen et al., 2022). Pb scavenges to both Fe oxyhydroxides ($Fe(OH)_3$) and MnO_2 (Bargar et al., 1997; Villalobos et al., 2005). However, particle scavenging of Pb by either authigenic particle phase seems to be relatively small within the UHL: a multiple linear regression using compositional fractions of both $Fe(OH)_3$ and MnO_2 also shows an insignificant relationship with K_d ($p > 0.05$).

Mn oxide scavenging likely decreases concentrations of almost all Theme 3 dissolved TEIs within the UHL, including dMn, dCo, dV and $d^{234}Th$. Interestingly, despite strong scavenging by MnO_2 within the UHL, dCu, $d^{230}Th$ and d^{231} Pa are categorized into Theme 1. The drawdown of these dissolved TEIs still occurs, but similar dissolved TEIs concentrations between the PML and UHL make scavenging signals harder to observe. This is further supported by high concentrations of pCu observed within the UHL (Figure S1 in Supporting Information S1). Overall, particle scavenging plays an important role in decreasing concentrations of many dissolved TEIs in all three themes, providing more insights into the mechanism of such characteristic distributions.

7. How Do We Expect Climate Change to Affect the Halocline

Recognizing the drastic changes ongoing in the Arctic with regards to surface air temperature, sea ice loss, reduction in terrestrial snow and ice, and permafrost thaw, we anticipate these trends will continue in the near future. Below, we consider the impacts these changes in the Arctic system may have on the chemistry of the Arctic halocline.

7.1. Northward Migration of the Seasonal Ice Zone

Arctic sea ice cover is already well into a rapid shift from perennial to seasonal over the pelagic ocean (Babb et al., 2022). That is, the seasonal ice zone (SIZ) has expanded from the shelves toward the pole, a trend that is expected to continue through this century (Brunette et al., 2019; Kwok, 2004, 2018; Newton et al., 2017, 2021; Pfirman et al., 2004; Rampal et al., 2009). This has impacted the structure of the upper water column through an increased mass of annual sea ice formation, longer open-water seasons, and increased rates of sea-ice drift (Kwok et al., 1998; Newton et al., 2017; Rampal et al., 2009). When the SIZ extends over the deep Arctic basins, increased ice formation in fall will lead to deepening of the winter mixed layer, and episodic (e.g., seasonal) degradation of the stratification between the UHL, AW and PML (Polyakov et al., 2017, 2020). Thus, the balance of isopycnal ventilation of the UHL (via shelf detrainment) and vertical ventilation (via brine-driven convection) are likely to shift toward the latter.

The Chukchi Sea, where much of the chemistry of the upper halocline is established, has recently seen especially rapid northward expansion of the SIZ. This has already led to changes in the timing of the spring bloom and phytoplankton community composition (Huntington et al., 2020; Lalande et al., 2021), consistent with a shift from benthic to pelagic communities. Current trends in the chemistry of the upper halocline waters are unknown, since these are the first halocline measurements for most of the parameters measured on GN01. In the near future, the fluxes of Theme 2 and Theme 3 elements will likely increase to the UHL due to enhanced sediment-water column exchange resulting from brine rejection and water column overturning during sea ice formation (Pacini et al., 2019; Weingartner et al., 1998), from increased frequency of storms (Ardyna et al., 2014), and enhanced internal wave energy facilitated by a longer open-water season (Rainville & Woodgate, 2009).

With respect to dissolved gasses, the sea ice cover is not an "air-tight lid", but it restricts air-sea fluxes, perhaps by about two thirds (Loose et al., 2011). As the SIZ expands (both in space and time) and the ice thins, concentrations of dissolved gasses in the mixed layer will further approach equilibrium with the Arctic atmosphere. If vertical ventilation of the halocline becomes more important (as discussed above), these changes will be propagated into the UHL.

7.2. Stratification and Relative Endmember Influence

The distributions of Theme 1 elements, which are dominated by diapycnal mixing, are set by gradients between the PML, BSI and AW concentrations. There is no reason to believe that the chemical composition of Atlantic Water inflow will change in the near future; however, shoaling of AW and weakening of the halocline have been observed along the Laptev Slope (Polyakov et al., 2017, 2020), which may shift the concentrations of Theme 1 elements in the halocline by changing the relative magnitude of the Atlantic endmember. Changes in the BSI are underway, with a persistent warming and freshening trend that is likely to shoal the PSW ventilation to the UHL (Woodgate and Peralta-Ferriz, 2021), weakening the halocline and, thereby, the subsurface nutrient and TEI reservoir. The thickness of the PML is also changing through time, in response to episodic changes in the surface wind-stresses (Hunkins & Whitehead, 1992; Proshutinsky & Johnson, 1997) as well as changes in the supply of freshwater from runoff and sea-ice melt (Newton et al., 2013; Proshutinsky et al., 2019). Therefore, while we do not expect the vertical structure of Theme 1 profiles to change, the relative magnitudes of the endmember influences, and the depth ranges of their dominance, are likely to shift incrementally.

7.3. Increase in Terrestrial Fluxes

Several climate-driven changes may increase the delivery of terrestrial-derived elements to the Arctic Ocean. River discharge is increasing (Holmes et al., 2021), resulting in an increase in ions associated with mineral weathering (Tank et al., 2023), which will likely have an impact on Theme 1 and Theme 3 elements. The northward retreat of sea ice allows for increased wind-driven mixing, water column turbulence, and surface wave

fetch (Rainville & Woodgate, 2009). These are increasing coastal erosion rates (Overeem et al., 2011) and likely causing an increased release of shelf sediment-derived elements into the overlying water column (Kipp et al., 2018). Further, aeolian deposition over open water will result in more sediment accumulation directly to the shelves, rather than to the surface of sea ice. Historically, dust has accumulated on the ice over several years, and is then deposited into the water column where the ice melts–mostly over the shelf seas and along the East Greenland Current (Newton et al., 2017). We are therefore likely to see increased particle supply from local atmospheric deposition in addition to sea ice transport (Pernov et al., 2022). Together, these changes are likely to impact the concentration of Theme 2 (and potentially Theme 3) elements in the UHL; concentrations of elements with a terrestrial source will likely increase.

Rising air and sea temperatures are also thawing permafrost (Luo et al., 2016). The subsea and above-ground permafrost that surrounds the Arctic Ocean currently acts as a reservoir of carbon, nutrients, and TEIs (Frey & McClelland, 2009; Schuur et al., 2008), so the thawing of permafrost results in increased concentrations of these liberated solutes in rivers (Feng et al., 2013; Frey & McClelland, 2009). Higher permafrost-derived solute concentrations in rivers are likely to have the greatest impact on Theme 1 elements, though this could also impact Theme 2 and 3 elements through alterations in the biogeochemical cycling of elements following delivery to the shelf seas.

Permafrost-derived solutes can also be transported to the coastal ocean via submarine groundwater discharge. Although permafrost likely acts as a physical barrier to groundwater flow across much of the Arctic, active submarine groundwater discharge has been documented in the Laptev Sea (Charkin et al., 2017) and is likely to increase in the future as permafrost continues to thaw (Walvoord et al., 2012). Because submarine groundwater discharge can extend out onto the continental shelf, this has the potential to impact the relative concentrations and biogeochemical cycling of all three types of elements discussed here. However, permafrost thaw is slow (~cm/y; Luo et al., 2016), and the signal of permafrost-derived solutes can be difficult to identify following dilution in rivers and the coastal ocean (e.g., Francis et al., 2023). It is therefore unlikely that we will be able to attribute significant changes in UHL chemistry to permafrost-driven shifts in the river- or shelf-cycling of elements in the near term. These potential changes may become more important in the future as degradation becomes more widespread and/or the rate of thaw increases.

8. Conclusions and Further Considerations

We have shown here that minor trace chemical constituents' diverse sources and behaviors can be leveraged to elucidate supply to and internal cycling in the halocline. The Chukchi shelf is an important modifier of the so-called “Pacific signal” of the halocline and many trace constituents are added to halocline waters during exposure to the shelves. In addition, biophysical processes over the shelves are highly variable spatially and seasonally, and they are undergoing a regime shift as the Arctic warms. Tracers in the upper halocline are integrative measures of those changes. Thus they provide an efficient way to track changes over both the shelf seas and the pelagic basins, where continuous monitoring is rare due to the very high costs of seagoing operations in remote areas.

An ongoing question into the utility of TEIs in the Arctic Ocean regards whether different shelf regions imprint distinct geochemical characteristics on the overlying waters (Alkire et al., 2019; Guay & Falkner, 1997). Certainly, there are enough observations in the Chukchi and Barents Seas to indicate that the shelf systems can be quite different from each other. Yet there are not enough observations along the East Siberian Sea to determine if there are distinct signatures between the Chukchi and East Siberian Sea, which are both shallow (<50 m) shelf systems. We approached this question by mapping our data as UHL (by isopycnal) averages (Figures S4–S6 in Supporting Information S1); ultimately, concentrations alone are not distinct between the Makarov and Canada Basin UHL. Our work characterizes the distributions of these TEIs, but further synthesis regarding elemental ratios may elucidate differences between the halocline across the Amerasian Basin (Alkire et al., 2019).

Climate-driven changes in the chemistry and ventilation of the halocline will propagate through the Arctic Ocean with lags commensurate with the mean transit times between water sources and sampling points. For the UHL, those times range from a year up to about 20 years. Unfortunately, we have already missed the window of opportunity to get a pre-regime-shift baseline. The data from the Arctic GEOTRACES campaigns are nonetheless an essential initial survey against which to measure the response of the Arctic Ocean to ongoing climate change. Given the timescales of transit and changes (both those evident in the historical record and those forced by current

warming trends), continued high-resolution monitoring of Arctic Ocean chemistry on sub-decadal timescales will be vital for assessing changes.

Data Availability Statement

All data are available via the GEOTRACES IDP (housed at BODC), BCO-DMO, or the CCHDO data repository. This study used several data sets generated during the 2015 US GEOTRACES Campaign in the Amerasian Basin of the Arctic Ocean (see Section 2 for more detail). Data sets and methodologies have been previously published and, thus, we did not extensively report on methods in the manuscript. Table 2 indicates where data may be found and what methods were used for both sampling and analysis.

Acknowledgments

The authors gratefully acknowledge the captain and crew on the USCGC Healy for their invaluable support on the 2015 Arctic GEOTRACES cruise. We acknowledge assistance in sample collection and processing from supertechs Gabrielle Weiss and Simone Moos, as well as leadership and direction by chief scientists Bill Landing and Dave Kadko. The US GEOTRACES Program office supported the synthesis work done in this project (National Science Foundation, Division of Ocean Sciences Grant Number 1536294 awarded to R. F. Anderson). Individual sample sets were funded by NSF-OCE. Further information on Grant funding can be found on the BCO-DMO website as well as in individual publications. The International GEOTRACES Programme is possible in part thanks to the support from the U.S. National Science Foundation (Grant OCE-2140395) to the Scientific Committee on Oceanic Research (SCOR).

References

Aagaard, K., & Carmack, E. C. (1994). The Arctic Ocean and climate: A perspective. In *The Polar Oceans and Their Role in Shaping the Global Environment* (pp. 5–20). American Geophysical Union (AGU). https://doi.org/10.1029/GM085p0005

Aagaard, K., Coachman, L. K., & Carmack, E. (1981). On the halocline of the Arctic Ocean. Deep sea Research Part A. *Oceanographic Research Papers*, *28*(6), 529–545. https://doi.org/10.1016/0198-0149(81)90115-1

Agather, A. M., Bowman, K. L., Lamborg, C. H., & Hammerschmidt, C. R. (2019). Distribution of mercury species in the western Arctic Ocean (U.S. GEOTRACES GN01). *Marine Chemistry*, *216*, 103686. https://doi.org/10.1016/j.marchem.2019.103686

Alkire, M. B., Rember, R., & Polyakov, I. (2019). Discrepancy in the identification of the Atlantic/Pacific front in the central Arctic Ocean: NO versus nutrient relationships. *Geophysical Research Letters*, *46*(7), 3843–3852. https://doi.org/10.1029/2018GL081837

Amon, R. M., Budéus, G., & Meon, B. (2003). Dissolved organic carbon distribution and origin in the Nordic seas: Exchanges with the Arctic Ocean and the North Atlantic. *Journal of Geophysical Research*, *108*(C7), 3221. https://doi.org/10.1029/2002JC001594

Anderson, L. G., Andersson, P. S., Björk, G., Peter Jones, E., Jutterström, S., & Wåhlström, I. (2013). Source and formation of the upper halocline of the Arctic Ocean. *Journal of Geophysical Research: Oceans*, *118*(1), 410–421. https://doi.org/10.1029/2012JC008291

Anderson, L. G., Tanhua, T., Björk, G., Hjalmarsson, S., Jones, E. P., Jutterström, S., et al. (2010). Arctic ocean shelf–basin interaction: An active continental shelf CO2 pump and its impact on the degree of calcium carbonate solubility. *Deep Sea Research Part I: Oceanographic Research Papers*, *57*(7), 869–879. https://doi.org/10.1016/j.dsr.2010.03.012

Anderson, R. F., Fleisher, M. Q., Robinson, L. F., Edwards, R. L., Hoff, J. A., Moran, S. B., et al. (2012). GEOTRACES intercalibration of 230Th, 232Th, 231Pa, and prospects for 10Be. *Limnology and Oceanography: Methods*, *10*(4), 179–213. https://doi.org/10.4319/lom.2012.10.179

Ardyna, M., Babin, M., Gosselin, M., Devred, E., Rainville, L., & Tremblay, J.-É. (2014). Recent Arctic Ocean sea ice loss triggers novel fall phytoplankton blooms. *Geophysical Research Letters*, *41*(17), 6207–6212. https://doi.org/10.1002/2014GL061047

Arrigo, K. R., & van Dijken, G. L. (2011). Secular trends in Arctic Ocean net primary production. *Journal of Geophysical Research*, *116*(C9), C09011. https://doi.org/10.1029/2011JC007151

Babb, D. G., Galley, R. J., Howell, S. E. L., Landy, J. C., Stroeve, J. C., & Barber, D. G. (2022). Increasing multiyear sea ice loss in the Beaufort Sea: A new export pathway for the diminishing multiyear ice cover of the Arctic Ocean. *Geophysical Research Letters*, *49*(9), e2021GL097595. https://doi.org/10.1029/2021GL097595

Bacon, M. P., & Anderson, R. F. (1982). Distribution of thorium isotopes between dissolved and particulate forms in the deep sea. *Journal of Geophysical Research*, *87*(C3), 2045–2056. https://doi.org/10.1029/JC087iC03p02045

Bam, W., Maiti, K., Baskaran, M., Krupp, K., Lam, P. J., & Xiang, Y. (2020). Variability in 210Pb and 210Po partition coefficients (Kd) along the US GEOTRACES Arctic transect. *Marine Chemistry*, *219*, 103749. https://doi.org/10.1016/j.marchem.2020.103749

Bargar, J. R., Brown, G. E., & Parks, G. A. (1997). Surface complexation of Pb(II) at oxide-water interfaces: II. XAFS and bond-valence determination of mononuclear Pb(II) sorption products and surface functional groups on iron oxides. *Geochimica et Cosmochimica Acta*, *61*(13), 2639–2652. https://doi.org/10.1016/S0016-7037(97)00125-7

Bates, N. R., Moran, S. B., Hansell, D. A., & Mathis, J. T. (2006). An increasing CO2 sink in the Arctic Ocean due to sea-ice loss. *Geophysical Research Letters*, *33*(23), L23609. https://doi.org/10.1029/2006GL027028

Bauch, D., Polyak, L., & Ortiz, J. D. (2015). A baseline for the vertical distribution of the stable carbon isotopes of dissolved inorganic carbon (δ13CDIC) in the Arctic Ocean. *Arktos*, *1*(1), 15. https://doi.org/10.1007/s41063-015-0001-0

Bourbonnais, A., & Altabet, M. (2021). Nitrous oxide concentration, stable isotope and isotopomer data for the GEOTRACES (an international study of the marine biogeochemical cycles of trace elements and isotopes) arctic section (summer 2015) [Dataset]. *Arctic Data Center*. https://doi.org/10.18739/A2N58CM9S

Bourbonnais, A., Chang, B. X., Sonnerup, R. E., Doney, S. C., & Altabet, M. A. (2023). Marine N2O cycling from high spatial resolution concentration, stable isotopic and isotopomer measurements along a meridional transect in the eastern Pacific Ocean. *Frontiers in Marine Science*, *10*, 1137064. https://doi.org/10.3389/fmars.2023.1137064

Bourbonnais, A., Letscher, R. T., Bange, H. W., Échevin, V., Larkum, J., Mohn, J., et al. (2017). N_2O production and consumption from stable isotopic and concentration data in the Peruvian coastal upwelling system: N_2O production and consumption off Peru. *Global Biogeochemical Cycles*, *31*(4), 678–698. https://doi.org/10.1002/2016GB005567

Bowman, K. L., Lamborg, C. H., & Agather, A. M. (2020). A global perspective on mercury cycling in the ocean. *Science of the Total Environment*, *710*, 136166. https://doi.org/10.1016/j.scitotenv.2019.136166

Boyle, E. A., Lee, J.-M., Echegoyen, Y., Noble, A., Moos, S., Carrasco, G., et al. (2014). Anthropogenic lead emissions in the ocean: The evolving global experiment. *Oceanography*, *27*(1), 69–75. https://doi.org/10.5670/oceanog.2014.10

Brown, K. A., McLaughlin, F., Tortell, P. D., Yamamoto-Kawai, M., & Francois, R. (2016). Sources of dissolved inorganic carbon to the Canada Basin halocline: A multitracer study. *Journal of Geophysical Research: Oceans*, *121*(5), 2918–2936. https://doi.org/10.1002/2015JC011535

Bruland, K. W., Middag, R., & Lohan, M. C. (2014). 8.2 - controls of trace metals in seawater. In H. D. Holland & K. K. Turekian (Eds.), *Treatise on Geochemistry* (2nd ed., pp. 19–51). Elsevier.

Brunette, C., Tremblay, B., & Newton, R. (2019). Winter coastal divergence as a predictor for the minimum sea ice extent in the Laptev Sea. *Journal of Climate*, *32*(4), 1063–1080. https://doi.org/10.1175/JCLI-D-18-0169.1

Brzezinski, M. A., Closset, I., Jones, J. L., de Souza, G. F., & Maden, C. (2021). New constraints on the physical and biological controls on the silicon isotopic composition of the Arctic Ocean. *Frontiers in Marine Science*, *8*. https://doi.org/10.3389/fmars.2021.699762

Bullister, J. L., & Warner, M. J. (2017). Atmospheric histories (1765-2022) for CFC-11, CFC-12, CFC-113, CCl4, SF6 and N2O (NCEI Accession 0164584) [Dataset]. *NOAA National Centers for Environmental Information*. https://doi.org/10.3334/CDIAC/OTG.CFC_ATM_HIST_2015

Bundy, R. M., Tagliabue, A., Hawco, N. J., Morton, P. L., Twining, B. S., Hatta, M., et al. (2020). Elevated sources of cobalt in the Arctic Ocean. *Biogeosciences*, *17*(19), 4745–4767. https://doi.org/10.5194/bg-17-4745-2020

Carter, B. R., Radich, J. A., Doyle, H. L., & Dickson, A. G. (2013). An automated system for spectrophotometric seawater pH measurements: Automated spectrophotometric pH measurement. *Limnology and Oceanography: Methods*, *11*(1), 16–27. https://doi.org/10.4319/lom.2013.11.16

CCHDO Hydrographic Data Office. (2023). CCHDO hydrographic data archive [Dataset]. In *CCHDO Hydrographic Data Archive*. UC San Diego Library Digital Collections. https://doi.org/10.7942/C2MW25

Chang, B. X., & Devol, A. H. (2009). Seasonal and spatial patterns of sedimentary denitrification rates in the Chukchi sea. *Deep Sea Research Part II: Topical Studies in Oceanography*, *56*(17), 1339–1350. https://doi.org/10.1016/j.dsr2.2008.10.024

Charette, M. A., Kipp, L. E., Jensen, L. T., Dabrowski, J. S., Whitmore, L. M., Fitzsimmons, J. N., et al. (2020). The transpolar drift as a source of riverine and shelf-derived trace elements to the central Arctic Ocean. *Journal of Geophysical Research: Oceans*, *125*(5), e2019JC015920. https://doi.org/10.1029/2019jc015920

Charkin, A. N., Rutgers Van Der Loeff, M., Shakhova, N. E., Gustafsson, Ö., Dudarev, O. V., Cherepnev, M. S., et al. (2017). Discovery and characterization of submarine groundwater discharge in the siberian arctic seas: A case study in the buor-khaya gulf, Laptev Sea. *The Cryosphere*, *11*(5), 2305–2327. https://doi.org/10.5194/tc-11-2305-2017

Chmiel, R., Lanning, N., Laubach, A., Lee, J.-M., Fitzsimmons, J., Hatta, M., et al. (2022). Major processes of the dissolved cobalt cycle in the North and equatorial Pacific Ocean. *Biogeosciences*, *19*(9), 2365–2395. https://doi.org/10.5194/bg-19-2365-2022

Cid, A. P., Nakatsuka, S., & Sohrin, Y. (2012). Stoichiometry among bioactive trace metals in the Chukchi and Beaufort Seas. *Journal of Oceanography*, *68*(6), 985–1001. https://doi.org/10.1007/s10872-012-0150-8

Codispoti, A., & Owens, T. G. (1975). Nutrient transports through Lancaster Sound in relation to the Arctic Ocean's reactive silicate budget and the outflow of Bering Strait waters. *Limnology & Oceanography*, *20*(1), 115–119. https://doi.org/10.4319/lo.1975.20.1.0115

Colombo, M., Jackson, S. L., Cullen, J. T., & Orians, K. J. (2020). Dissolved iron and manganese in the Canadian Arctic Ocean: On the biogeochemical processes controlling their distributions. *Geochimica et Cosmochimica Acta*, *277*, 150–174. https://doi.org/10.1016/j.gca.2020.03.012

Colombo, M., Rogalla, B., Myers, P. G., Allen, S. E., & Orians, K. J. (2019). Tracing dissolved lead sources in the Canadian arctic: Insights from the Canadian GEOTRACES program. *ACS Earth and Space Chemistry*, *3*(7), 1302–1314. https://doi.org/10.1021/acsearthspacechem.9b00083

Cooper, L. W., Benner, R., McClelland, J. W., Peterson, B. J., Holmes, R. M., Raymond, P. A., et al. (2005). Linkages among runoff, dissolved organic carbon, and the stable oxygen isotope composition of seawater and other water mass indicators in the Arctic Ocean. *Journal of Geophysical Research*, *110*(G2), G02013. https://doi.org/10.1029/2005JG000031

Cooper, L. W., McClelland, J. W., Holmes, R. M., Raymond, P. A., Gibson, J. J., Guay, C. K., & Peterson, B. J. (2008). Flow-weighted values of runoff tracers (δ18O, DOC, Ba, alkalinity) from the six largest Arctic rivers. *Geophysical Research Letters*, *35*(18), L18606. https://doi.org/10.1029/2008GL035007

Corlett, W. B., & Pickart, R. S. (2017). The Chukchi slope current. *Progress in Oceanography*, *153*, 50–65. https://doi.org/10.1016/j.pocean.2017.04.005

Cui, X., Lamborg, C. H., Hammerschmidt, C. R., Xiang, Y., & Lam, P. J. (2021). The effect of particle composition and concentration on the partitioning coefficient for mercury in three Ocean Basins. *Frontiers in Environmental Chemistry*, *2*. https://doi.org/10.3389/fenvc.2021.660267

Cutter, G., Andersson, P. S., Codispoti, L. A., Croot, P., Francois, R., Lohan, M., et al. (2014). Sampling and Sample-handling Protocols for GEOTRACES Cruises, Version 2. Retrieved from http://www.geotraces.org/library-88/scientific-publications/reports/169-sampling-and-sample-handling-protocols-for-geotraces-cruises

Dastoor, A., Angot, H., Bieser, J., Christensen, J. H., Douglas, T. A., Heimbürger-Boavida, L.-E., et al. (2022). Arctic mercury cycling. *Nature Reviews Earth and Environment*, *3*(4), 270–286. https://doi.org/10.1038/s43017-022-00269-w

Dickson, A. G., Sabine, C. L., & Christian, J. R. (2007). *Guide to best practices for ocean CO2 measurements*. North Pacific Marine Science Organization.

Dmitrenko, I. A., Rudels, B., Kirillov, S. A., Aksenov, Y. O., Lien, V. S., Ivanov, V. V., et al. (2015). Atlantic water flow into the Arctic Ocean through the St. Anna trough in the northern Kara sea: Atlantic water flow to the Arctic Ocean. *Journal of Geophysical Research: Oceans*, *120*(7), 5158–5178. https://doi.org/10.1002/2015JC010804

Dodd, P. A., Rabe, B., Hansen, E., Falck, E., Mackensen, A., Rohling, E., et al. (2012). The freshwater composition of the Fram Strait outflow derived from a decade of tracer measurements. *Journal of Geophysical Research*, *117*(C11), C11005. https://doi.org/10.1029/2012JC008011

Ekwurzel, B., Schlosser, P., Mortlock, R. A., Fairbanks, R. G., & Swift, J. H. (2001). River runoff, sea ice meltwater, and Pacific water distribution and mean residence times in the Arctic Ocean. *Journal of Geophysical Research*, *106*(C5), 9075–9092. https://doi.org/10.1029/1999JC000024

Else, B. G. T., Galley, R. J., Lansard, B., Barber, D. G., Brown, K., Miller, L. A., et al. (2013). Further observations of a decreasing atmospheric CO2 uptake capacity in the Canada Basin (Arctic Ocean) due to sea ice loss. *Geophysical Research Letters*, *40*(6), 1132–1137. https://doi.org/10.1002/grl.50268

Feng, X., Vonk, J. E., Van Dongen, B. E., Gustafsson, Ö., Semiletov, I. P., Dudarev, O. V., et al. (2013). Differential mobilization of terrestrial carbon pools in Eurasian Arctic river basins. *Proceedings of the National Academy of Sciences*, *110*(35), 14168–14173. https://doi.org/10.1073/pnas.1307031110

Fenwick, L., Capelle, D., Damm, E., Zimmermann, S., Williams, W. J., Vagle, S., & Tortell, P. D. (2017). Methane and nitrous oxide distributions across the North American Arctic Ocean during summer, 2015: CH_4 and N_2O distributions in Arctic Ocean. *Journal of Geophysical Research: Oceans*, *122*(1), 390–412. https://doi.org/10.1002/2016JC012493

Fine, R. A. (2011). Observations of CFCs and SF6 as ocean tracers. *Annual Review of Marine Science*, *3*(1), 173–195. https://doi.org/10.1146/annurev.marine.010908.163933

Francis, A., Ganeshram, R. S., Tuerena, R. E., Spencer, R. G. M., Holmes, R. M., Rogers, J. A., & Mahaffey, C. (2023). Permafrost degradation and nitrogen cycling in arctic rivers: Insights from stable nitrogen isotope studies. *Biogeosciences*, *20*(2), 365–382. https://doi.org/10.5194/bg-20-365-2023

Frey, K. E., & McClelland, J. W. (2009). Impacts of permafrost degradation on arctic river biogeochemistry. *Hydrological Processes*, *23*(1), 169–182. https://doi.org/10.1002/hyp.7196

Fripiat, F., Declercq, M., Sapart, C. J., Anderson, L. G., Bruechert, V., Deman, F., et al. (2018). Influence of the bordering shelves on nutrient distribution in the Arctic halocline inferred from water column nitrate isotopes. *Limnology & Oceanography*, *63*(5), 2154–2170. https://doi.org/10.1002/lno.10930

Gdaniec, S., Roy-Barman, M., Levier, M., Valk, O., van der Loeff, M. R., Foliot, L., et al. (2020). 231Pa and 230Th in the Arctic Ocean: Implications for boundary scavenging and 231Pa230Th fractionation in the Eurasian Basin. *Chemical Geology*, *532*, 119380. https://doi.org/10.1016/j.chemgeo.2019.119380

GEOTRACES Intermediate Data Product Group. (2021). The GEOTRACES intermediate data product 2021 (IDP2021) [Dataset]. *NERC EDS British Oceanographic Data Centre NOC*. Retrieved from https://www.bodc.ac.uk/data/published_data_library/catalogue/10.5285/cf2d9ba9-d51d-3b7c-e053-8486abc0f5fd/

Gerringa, L. J. A., Rijkenberg, M. J. A., Slagter, H. A., Laan, P., Paffrath, R., Bauch, D., et al. (2021). Dissolved Cd, Co, Cu, Fe, Mn, Ni and Zn in the Arctic Ocean. *Journal of Geophysical Research: Oceans*, *126*(9), e2021JC017323. https://doi.org/10.1029/2021JC017323

Giesbrecht, K. E., & Varela, D. E. (2021). Summertime biogenic silica production and silicon limitation in the Pacific arctic region from 2006 to 2016. *Global Biogeochemical Cycles*, *35*(1). https://doi.org/10.1029/2020GB006629

Goldberg, E. D. (1954). Marine geochemistry 1. Chemical scavengers of the sea. *The Journal of Geology*, *62*(3), 249–265. https://doi.org/10.1086/626161

Granger, J., Prokopenko, M. G., Mordy, C. W., & Sigman, D. M. (2013). The proportion of remineralized nitrate on the ice-covered eastern Bering Sea shelf evidenced from the oxygen isotope ratio of nitrate. *Global Biogeochemical Cycles*, *27*(3), 962–971. https://doi.org/10.1002/gbc.20075

Granger, J., Prokopenko, M. G., Sigman, D. M., Mordy, C. W., Morse, Z. M., Morales, L. V., et al. (2011). Coupled nitrification-denitrification in sediment of the eastern Bering Sea shelf leads to 15N enrichment of fixed N in shelf waters. *Journal of Geophysical Research*, *116*(C11), C11006. https://doi.org/10.1029/2010JC006751

Granger, J., Sigman, D. M., Gagnon, J., Tremblay, J., & Mucci, A. (2018). On the properties of the arctic halocline and deep water masses of the Canada basin from nitrate isotope ratios. *Journal of Geophysical Research: Oceans*, *123*(8), 5443–5458. https://doi.org/10.1029/2018JC014110

Guay, C. K., & Falkner, K. (1997). Barium as a tracer of Arctic halocline and river waters. *Deep Sea Research Part II: Topical Studies in Oceanography*, *44*(8), 1543–1569. https://doi.org/10.1016/S0967-0645(97)00066-0

Halewood, E., Opalk, K., Custals, L., Carey, M., Hansell, D. A., & Carlson, C. A. (2022). GO-SHIP Repeat Hydrography: Determination of dissolved organic carbon (DOC) and total dissolved nitrogen (TDN) in seawater using High Temperature Combustion Analysis. *Methods, Front. Mar. Sci. - Ocean Observation*, *9*. https://doi.org/10.3389/fmars.2022.1061646

Hansell, D. A., Kadko, D., & Bates, N. R. (2004). Degradation of terrigenous dissolved organic carbon in the western Arctic Ocean. *Science*, *304*(5672), 858–861. https://doi.org/10.1126/science.1096175

Hansell, D. A., Whitledge, T. E., & Goering, J. J. (1993). Patterns of nitrate utilization and new production over the Bering-Chukchi shelf. *Continental Shelf Research*, *13*(5), 601–627. https://doi.org/10.1016/0278-4343(93)90096-G

Hayes, C. T., Anderson, R. F., Fleisher, M. Q., Vivancos, S. M., Lam, P. J., Ohnemus, D. C., et al. (2015). Intensity of Th and Pa scavenging partitioned by particle chemistry in the North Atlantic Ocean. *Marine Chemistry*, *170*, 49–60. https://doi.org/10.1016/j.marchem.2015.01.006

Hayes, C. T., Black, E. E., Anderson, R. F., Baskaran, M., Buesseler, K. O., Charette, M. A., et al. (2018). Flux of particulate elements in the North Atlantic ocean constrained by multiple radionuclides. *Global Biogeochemical Cycles*, *32*(12), 1738–1758. https://doi.org/10.1029/2018GB005994

He, X., Sun, L., Xie, Z., Huang, W., Long, N., Li, Z., & Xing, G. (2013). Sea ice in the Arctic Ocean: Role of shielding and consumption of methane. *Atmospheric Environment*, *67*, 8–13. https://doi.org/10.1016/j.atmosenv.2012.10.029

Hirota, A., Ijiri, A., Komatsu, D. D., Ohkubo, S. B., Nakagawa, F., & Tsunogai, U. (2009). Enrichment of nitrous oxide in the water columns in the area of the Bering and Chukchi Seas. *Marine Chemistry*, *116*(1), 47–53. https://doi.org/10.1016/j.marchem.2009.09.001

Ho, P., Lee, J.-M., Heller, M. I., Lam, P. J., & Shiller, A. M. (2018). The distribution of dissolved and particulate Mo and V along the U.S. GEOTRACES East Pacific Zonal Transect (GP16): The roles of oxides and biogenic particles in their distributions in the oxygen deficient zone and the hydrothermal plume. *Marine Chemistry*, *201*, 242–255. https://doi.org/10.1016/j.marchem.2017.12.003

Hoffmann, S. S., McManus, J. F., Curry, W. B., & Brown-Leger, L. S. (2013). Persistent export of 231Pa from the deep central Arctic Ocean over the past 35,000 years. *Nature*, *497*(7451), 603–606. https://doi.org/10.1038/nature12145

Holmes, R. M., Shiklomanov, A. I., Suslova, A., Tretiakov, M., McClelland, J. W., Scott, L., et al. (2021). NOAA Arctic Report Card 2021: River Discharge. https://doi.org/10.25923/ZEVF-AR65

Hood, E. M., Sabine, C. L., & Sloyan, B. M. (Eds.) (2010)., *GO-SHIP repeat hydrography manual: A collection of expert reports and guidelines*, *IOCCP Report Number 14, ICPO Publication Series Number 134. Retrieved from*. Retrieved from http://www.go-ship.org/HydroMan.html

Horner, T. J., Little, S. H., Conway, T. M., Farmer, J. R., Hertzberg, J. E., Janssen, D. J., et al. (2021). Bioactive trace metals and their isotopes as paleoproductivity proxies: An assessment using GEOTRACES-Era data. *Global Biogeochemical Cycles*, *35*(11), e2020GB006814. https://doi.org/10.1029/2020GB006814

Hunkins, K., & Whitehead, J. A. (1992). Laboratory simulation of exchange through Fram Strait. *Journal of Geophysical Research*, *97*(C7), 11299–11321. https://doi.org/10.1029/92JC00735

Huntington, H. P., Danielson, S. L., Wiese, F. K., Baker, M., Boveng, P., Citta, J. J., et al. (2020). Evidence suggests potential transformation of the Pacific Arctic ecosystem is underway. *Nature Climate Change*, *10*(4), 342–348. https://doi.org/10.1038/s41558-020-0695-2

Itoh, M., Pickart, R. S., Kikuchi, T., Fukamachi, Y., Ohshima, K. I., Simizu, D., et al. (2015). Water properties, heat and volume fluxes of Pacific water in Barrow Canyon during summer 2010. *Deep Sea Research Part I: Oceanographic Research Papers*, *102*, 43–54. https://doi.org/10.1016/j.dsr.2015.04.004

Jackson, J. M., Carmack, E. C., McLaughlin, F. A., Allen, S. E., & Ingram, R. G. (2010). Identification, characterization, and change of the near-surface temperature maximum in the Canada Basin, 1993–2008. *Journal of Geophysical Research*, *115*(C5), C05021. https://doi.org/10.1029/2009JC005265

Jacquot, J. E., & Moffett, J. W. (2015). Copper distribution and speciation across the international GEOTRACES section GA03. *Deep Sea Research Part II: Topical Studies in Oceanography*, *116*, 187–207. https://doi.org/10.1016/j.dsr2.2014.11.013

Jenkins, W. J., & Clarke, W. B. (1976). The distribution of 3He in the western Atlantic ocean. *Deep-Sea Research and Oceanographic Abstracts*, *23*(6), 481–494. https://doi.org/10.1016/0011-7471(76)90860-3

Jensen, L. T., Cullen, J. T., Jackson, S. L., Gerringa, L. J. A., Bauch, D., Middag, R., et al. (2022). A refinement of the processes controlling dissolved copper and nickel biogeochemistry: Insights from the Pan-arctic. *Journal of Geophysical Research: Oceans*, *127*(5), e2021JC018087. https://doi.org/10.1029/2021JC018087

Jensen, L. T., Morton, P., Twining, B. S., Heller, M. I., Hatta, M., Measures, C. I., et al. (2020). A comparison of marine Fe and Mn cycling: U.S. GEOTRACES GN01 western arctic case study. *Geochimica et Cosmochimica Acta*, *288*, 138–160. https://doi.org/10.1016/j.gca.2020.08.006

Jensen, L. T., Wyatt, N. J., Landing, W. M., & Fitzsimmons, J. N. (2020). Assessment of the stability, sorption, and exchangeability of marine dissolved and colloidal metals. *Marine Chemistry*, *220*, 103754. https://doi.org/10.1016/j.marchem.2020.103754

Jensen, L. T., Wyatt, N. J., Twining, B. S., Rauschenberg, S., Landing, W. M., Sherrell, R. M., & Fitzsimmons, J. N. (2019). Biogeochemical cycling of dissolved zinc in the western arctic (arctic GEOTRACES GN01). *Global Biogeochemical Cycles*, *33*(3), 343–369. https://doi.org/10.1029/2018GB005975

Ji, B. Y., Sandwith, Z. O., Williams, W. J., Diaconescu, O., Ji, R., Li, Y., et al. (2019). Variations in rates of biological production in the Beaufort gyre as the arctic changes: Rates from 2011 to 2016. *Journal of Geophysical Research: Oceans*, *124*(6), 3628–3644. https://doi.org/10.1029/2018JC014805

Jones, E. P., & Anderson, L. G. (1986). On the origin of the chemical properties of the Arctic Ocean halocline. *Journal of Geophysical Research*, *91*(C9), 10759–10767. https://doi.org/10.1029/JC091iC09p10759

Jones, E. P., Anderson, L. G., & Swift, J. H. (1998). Distribution of Atlantic and Pacific waters in the upper Arctic Ocean: Implications for circulation. *Geophysical Research Letters*, *25*(6), 765–768. https://doi.org/10.1029/98GL00464

Jones, E. P., & Coote, A. R. (1980). Nutrient distributions in the Canadian Archipelago: Indicators of summer water mass and flow characteristics. *Canadian Journal of Fisheries and Aquatic Sciences*, *37*(4), 589–599. https://doi.org/10.1139/f80-075

Jones, E. P., Swift, J. H., Anderson, L. G., Lipizer, M., Civitarese, G., Falkner, K. K., et al. (2003). Tracing Pacific water in the North Atlantic ocean. *Journal of Geophysical Research*, *108*(C4), 3116. https://doi.org/10.1029/2001JC001141

Juranek, L. W., Hales, B., Beaird, N. L., Goñi, M. A., Shroyer, E., Allen, J. G., & White, A. E. (2023). The importance of subsurface productivity in the Pacific arctic gateway as revealed by high-resolution biogeochemical surveys. *Journal of Geophysical Research: Oceans*, *128*(2), e2022JC019292. https://doi.org/10.1029/2022JC019292

Kipp, L. E., Charette, M. A., Moore, W. S., Henderson, P. B., & Rigor, I. G. (2018). Increased fluxes of shelf-derived materials to the central Arctic Ocean. *Science Advances*, *4*(1), eaao1302. https://doi.org/10.1126/sciadv.aao1302

Kipp, L. E., Kadko, D. C., Pickart, R. S., Henderson, P. B., Moore, W. S., & Charette, M. A. (2019). Shelf-Basin interactions and water mass residence times in the western Arctic Ocean: Insights provided by radium isotopes. *Journal of Geophysical Research: Oceans*, *124*(5), 3279–3297. https://doi.org/10.1029/2019JC014988

Kipp, L. E., Spall, M. A., Pickart, R. S., Kadko, D. C., Moore, W. S., Dabrowski, J. S., & Charette, M. A. (2020). Observational and modeling evidence of seasonal trends in sediment-derived material inputs to the Chukchi Sea. *Journal of Geophysical Research: Oceans*, *125*(5), e2019JC016007. https://doi.org/10.1029/2019JC016007

Kitidis, V., Upstill-Goddard, R. C., & Anderson, L. G. (2010). Methane and nitrous oxide in surface water along the North-west passage, Arctic Ocean. *Marine Chemistry*, *121*(1–4), 80–86. https://doi.org/10.1016/j.marchem.2010.03.006

Ko, Y. H., & Quay, P. D. (2020). Origin and accumulation of an anthropogenic CO_2 and^{13} C suess effect in the Arctic Ocean. *Global Biogeochemical Cycles*, *34*(2), e2019GB006423. https://doi.org/10.1029/2019GB006423

Kondo, Y., Obata, H., Hioki, N., Ooki, A., Nishino, S., Kikuchi, T., & Kuma, K. (2016). Transport of trace metals (Mn, Fe, Ni, Zn and Cd) in the western Arctic Ocean (Chukchi Sea and Canada basin) in late summer 2012. *Deep Sea Research Part I: Oceanographic Research Papers*, *116*, 236–252. https://doi.org/10.1016/j.dsr.2016.08.010

Kudo, K., Toyoda, S., Yamada, K., Yoshida, N., Sasano, D., Kosugi, N., et al. (2022). Source analysis of dissolved methane in Chukchi Sea and Bering Strait during summer–autumn of 2012 and 2013. *Marine Chemistry*, *243*, 104119. https://doi.org/10.1016/j.marchem.2022.104119

Kwok, R. (2004). Annual cycles of multiyear sea ice coverage of the Arctic Ocean: 1999–2003. *Journal of Geophysical Research*, *109*(C11), C11004. https://doi.org/10.1029/2003JC002238

Kwok, R. (2018). Arctic sea ice thickness, volume, and multiyear ice coverage: Losses and coupled variability (1958–2018). *Environmental Research Letters*, *13*(10), 105005. https://doi.org/10.1088/1748-9326/aae3ec

Kwok, R., Schweiger, A., Rothrock, D. A., Pang, S., & Kottmeier, C. (1998). Sea ice motion from satellite passive microwave imagery assessed with ERS SAR and buoy motions. *Journal of Geophysical Research*, *103*(C4), 8191–8214. https://doi.org/10.1029/97JC03334

Lalande, C., Grebmeier, J. M., McDonnell, A. M. P., Hopcroft, R. R., O'Daly, S., & Danielson, S. L. (2021). Impact of a warm anomaly in the Pacific Arctic region derived from time-series export fluxes. *PLoS One*, *16*(8), e0255837. https://doi.org/10.1371/journal.pone.0255837

Lam, P. J., Lee, J.-M., Heller, M. I., Mehic, S., Xiang, Y., & Bates, N. R. (2018). Size-fractionated distributions of suspended particle concentration and major phase composition from the U.S. GEOTRACES Eastern Pacific Zonal Transect (GP16). *The U.S.GEOTRACES Eastern Tropical Pacific Transect (GP16)*, *201*, 90–107. https://doi.org/10.1016/j.marchem.2017.08.013

Lamborg, C. H., Hammerschmidt, C. R., Gill, G. A., Mason, R. P., & Gichuki, S. (2012). An intercomparison of procedures for the determination of total mercury in seawater and recommendations regarding mercury speciation during GEOTRACES cruises. *Limnology and Oceanography: Methods*, *10*(2), 90–100. https://doi.org/10.4319/lom.2012.10.90

Lee, J.-M., Lam, P. J., Vivancos, S. M., Pavia, F. J., Anderson, R. F., Lu, Y., et al. (2021). Changing chemistry of particulate manganese in the near- and far-field hydrothermal plumes from 15°S East Pacific Rise and its influence on metal scavenging. *Geochimica et Cosmochimica Acta*, *300*, 95–118. https://doi.org/10.1016/j.gca.2021.02.020

Lehmann, N., Kienast, M., Granger, J., Bourbonnais, A., Altabet, M. A., & Tremblay, J.-É. (2019). Remote western arctic nutrients fuel remineralization in deep Baffin Bay. *Global Biogeochemical Cycles*, *33*(6), 649–667. https://doi.org/10.1029/2018GB006134

Lehmann, N., Kienast, M., Granger, J., & Tremblay, J.-É. (2022). Physical and biogeochemical influences on nutrients through the Canadian arctic Archipelago: Insights from nitrate isotope ratios. *Journal of Geophysical Research: Oceans*, *127*(3), e2021JC018179. https://doi.org/10.1029/2021JC018179

Lerner, P., Marchal, O., Lam, P. J., Buesseler, K., & Charette, M. (2017). Kinetics of thorium and particle cycling along the U.S. GEOTRACES North Atlantic transect. *Deep Sea Research Part I: Oceanographic Research Papers*, *125*, 106–128. https://doi.org/10.1016/j.dsr.2017.05.003

Letscher, R. T., Hansell, D. A., & Kadko, D. (2011). Rapid removal of terrigenous dissolved organic carbon over the Eurasian shelves of the Arctic Ocean. *Marine Chemistry*, *123*(1–4), 78–87. https://doi.org/10.1016/j.marchem.2010.10.002

Li, H., & Fedorov, A. V. (2021). Persistent freshening of the Arctic Ocean and changes in the North Atlantic salinity caused by Arctic sea ice decline. *Climate Dynamics*, *57*(11), 2995–3013. https://doi.org/10.1007/s00382-021-05850-5

Li, M., Pickart, R. S., Spall, M. A., Weingartner, T. J., Lin, P., Moore, G. W. K., & Qi, Y. (2019). Circulation of the Chukchi Sea shelfbreak and slope from moored timeseries. *Progress in Oceanography*, *172*, 14–33. https://doi.org/10.1016/j.pocean.2019.01.002

Li, Y., Zhan, L., Zhang, J., Chen, L., Chen, J., & Zhuang, Y. (2017). A significant methane source over the Chukchi Sea shelf and its sources. *Continental Shelf Research*, *148*, 150–158. https://doi.org/10.1016/j.csr.2017.08.019

Liguori, B. T. P., Ehlert, C., Nöthig, E., Ooijen, J. C., & Pahnke, K. (2021). The transpolar drift influence on the Arctic Ocean silicon cycle. *Journal of Geophysical Research: Oceans*, *126*(11), e2021JC017352. https://doi.org/10.1029/2021JC017352

Loose, B., Schlosser, P., Perovich, D., Ringelberg, D., Ho, D. t., Takahashi, T., et al. (2011). Gas diffusion through columnar laboratory sea ice: Implications for mixed-layer ventilation of CO2 in the seasonal ice zone. *Tellus B: Chemical and Physical Meteorology*, *63*(1), 23–39. https://doi.org/10.1111/j.1600-0889.2010.00506.x

Lorenson, T. D., Greinert, J., & Coffin, R. B. (2016). Dissolved methane in the Beaufort Sea and the Arctic Ocean, 1992–2009; sources and atmospheric flux. *Limnology & Oceanography*, *61*(S1), S300–S323. https://doi.org/10.1002/lno.10457

Lowry, K. E., Pickart, R. S., Mills, M. M., Brown, Z. W., van Dijken, G. L., Bates, N. R., & Arrigo, K. R. (2015). The influence of winter water on phytoplankton blooms in the Chukchi Sea. *Deep Sea Research Part II: Topical Studies in Oceanography*, *118*, 53–72. https://doi.org/10.1016/j.dsr2.2015.06.006

Lucas, L. L., & Unterweger, M. P. (2000). Comprehensive review and critical evaluation of the half-life of tritium. *Journal of Research of the National Institute of Standards and Technology*, *105*(4), 541–549. https://doi.org/10.6028/jres.105.043

Ludin, A., Wepperning, R., Bönisch, G., & Schlosser, P. (1997). Mass spectrometric measurement of helium isotopes and tritium in water samples. *Technical Report, Lamont-Doherty Earth Observatory*.

Luo, D., Wu, Q., Jin, H., Marchenko, S. S., Lü, L., & Gao, S. (2016). Recent changes in the active layer thickness across the northern hemisphere. *Environmental Earth Sciences*, *75*(7), 555. https://doi.org/10.1007/s12665-015-5229-2

Manning, C. C. M., Zheng, Z., Fenwick, L., McCulloch, R. D., Damm, E., Izett, R. W., et al. (2022). Interannual variability in methane and nitrous oxide concentrations and sea-air fluxes across the North American Arctic Ocean (2015–2019). *Global Biogeochemical Cycles*, *36*(4), e2021GB007185. https://doi.org/10.1029/2021GB007185

Marsay, C. M., Kadko, D., Landing, W. M., Morton, P. L., Summers, B. A., & Buck, C. S. (2018). Concentrations, provenance and flux of aerosol trace elements during US GEOTRACES Western Arctic cruise GN01. *Chemical Geology*, *502*, 1–14. https://doi.org/10.1016/j.chemgeo.2018.06.007

Mason, R. P., Choi, A. L., Fitzgerald, W. F., Hammerschmidt, C. R., Lamborg, C. H., Soerensen, A. L., & Sunderland, E. M. (2012). Mercury biogeochemical cycling in the ocean and policy implications. *Environmental Research*, *119*, 101–117. https://doi.org/10.1016/j.envres.2012.03.013

Masson-Delmotte, V., Zhai, P., Pirani, A., Connors, S. L., Péan, C., Chen, Y., et al. (2021). *IPCC, 2021: Climate Change 2021: The Physical Science Basis. Contribution of Working Group I to the Sixth Assessment Report of the Intergovernmental Panel on Climate Change*. Cambridge University Press. https://doi.org/10.1017/9781009157896.2391

Mathis, J. T., Hansell, D. A., & Bates, N. R. (2005). Strong hydrographic controls on spatial and seasonal variability of dissolved organic carbon in the Chukchi Sea. *Deep Sea Research Part II: Topical Studies in Oceanography*, *52*(24), 3245–3258. https://doi.org/10.1016/j.dsr2.2005.10.002

Mathis, J. T., Pickart, R. S., Hansell, D. A., Kadko, D., & Bates, N. R. (2007). Eddy transport of organic carbon and nutrients from the Chukchi Shelf: Impact on the upper halocline of the western Arctic Ocean. *Journal of Geophysical Research*, *112*(C5), C05011. https://doi.org/10.1029/2006JC003899

McAlister, J. A., & Orians, K. J. (2015). Dissolved gallium in the Beaufort Sea of the western Arctic Ocean: A GEOTRACES cruise in the international polar year. *Marine Chemistry*, *177*, 101–109. https://doi.org/10.1016/j.marchem.2015.05.007

McLaughlin, F. A., & Carmack, E. C. (2010). Deepening of the nutricline and chlorophyll maximum in the Canada basin interior, 2003-2009: Deepening of the Canada basin nutricline. *Geophysical Research Letters*, *37*(24). https://doi.org/10.1029/2010GL045459

Middag, R., de Baar, H. J. W., Bruland, K. W., & van Heuven, S. M. A. C. (2020). The distribution of nickel in the west-Atlantic ocean, its relationship with phosphate and a comparison to cadmium and zinc. *Frontiers in Marine Science*, *7*. https://doi.org/10.3389/fmars.2020.00105

Moore, R. M., Lowings, M. G., & Tan, F. C. (1983). Geochemical profiles in the central Arctic Ocean: Their relation to freezing and shallow circulation. *Journal of Geophysical Research*, *88*(C4), 2667–2674. https://doi.org/10.1029/JC088iC04p02667

Mordy, C. W., Eisner, L., Kearney, K., Kimmel, D., Lomas, M. W., Mier, K., et al. (2021). Spatiotemporal variability of the nitrogen deficit in bottom waters on the eastern Bering Sea shelf. *Continental Shelf Research*, *224*, 104423. https://doi.org/10.1016/j.csr.2021.104423

Newton, R., Pfirman, S., Tremblay, B., & DeRepentigny, P. (2017). Increasing transnational sea-ice exchange in a changing Arctic Ocean. *Earth's Future*, *5*(6), 633–647. https://doi.org/10.1002/2016EF000500

Newton, R., Pfirman, S., Tremblay, L. B., & DeRepentigny, P. (2021). Defining the "ice shed" of the Arctic Ocean's last ice area and its future evolution. *Earth's Future*, *9*(9), e2021EF001988. https://doi.org/10.1029/2021EF001988

Newton, R., Schlosser, P., Martinson, D. G., & Maslowski, W. (2008). Freshwater distribution in the Arctic Ocean: Simulation with a high-resolution model and model-data comparison. *Journal of Geophysical Research*, *113*(C5), C05024. https://doi.org/10.1029/2007JC004111

Newton, R., Schlosser, P., Mortlock, R., Swift, J., & MacDonald, R. (2013). Canadian basin freshwater sources and changes: Results from the 2005 Arctic Ocean section: AOS 2005 freshwater sources and changes. *Journal of Geophysical Research: Oceans*, *118*(4), 2133–2154. https://doi.org/10.1002/jgrc.20101

Nishino, S., Kikuchi, T., Fujiwara, A., Hirawake, T., & Aoyama, M. (2016). Water mass characteristics and their temporal changes in a biological hotspot in the southern Chukchi Sea. *Biogeosciences*, *13*(8), 2563–2578. https://doi.org/10.5194/bg-13-2563-2016

Not, C., Brown, K., Ghaleb, B., & Hillaire-Marcel, C. (2012). Conservative behavior of uranium vs. salinity in Arctic sea ice and brine. *Marine Chemistry*, *130–131*, 33–39. https://doi.org/10.1016/j.marchem.2011.12.005

Nozaki, Y., Zhang, J., & Takeda, A. (1997). 2I0Pb and210Po in the equatorial pacific and the Bering Sea: The effects of biological productivity and boundary scavenging. *Deep Sea Research Part II: Topical Studies in Oceanography*, *44*(9), 2203–2220. https://doi.org/10.1016/S0967-0645(97)00024-6

Ohnemus, D. C., Rauschenberg, S., Cutter, G. A., Fitzsimmons, J. N., Sherrell, R. M., & Twining, B. S. (2017). Elevated trace metal content of prokaryotic communities associated with marine oxygen deficient zones. *Limnology & Oceanography*, *62*(1), 3–25. https://doi.org/10.1002/lno.10363

Orians, K. J., & Bruland, K. W. (1988). The marine geochemistry of dissolved gallium: A comparison with dissolved aluminum. *Geochimica et Cosmochimica Acta*, *52*(12), 2955–2962. https://doi.org/10.1016/0016-7037(88)90160-3

Overeem, I., Anderson, R. S., Wobus, C. W., Clow, G. D., Urban, F. E., & Matell, N. (2011). Sea ice loss enhances wave action at the Arctic coast. *Geophysical Research Letters*, *38*(17), L17503. https://doi.org/10.1029/2011GL048681

Owens, N. J. P., Law, C. S., Mantoura, R. F. C., Burkill, P. H., & Llewellyn, C. A. (1991). Methane flux to the atmosphere from the Arabian sea. *Nature*, *354*(6351), 293–296. https://doi.org/10.1038/354293a0

Owens, S. A., Buesseler, K. O., & Sims, K. W. W. (2011). Re-evaluating the 238U-salinity relationship in seawater: Implications for the 238U–234Th disequilibrium method. *Marine Chemistry*, *127*(1), 31–39. https://doi.org/10.1016/j.marchem.2011.07.005

Pacini, A., Moore, G. W. K., Pickart, R. S., Nobre, C., Bahr, F., Våge, K., & Arrigo, K. R. (2019). Characteristics and transformation of Pacific winter water on the Chukchi Sea shelf in late spring. *Journal of Geophysical Research: Oceans*, *124*(10), 7153–7177. https://doi.org/10.1029/2019JC015261

Pasqualini, A., Schlosser, P., Newton, R., Smethie, W. M., Jr., & Friedrich, R. (2024). A multi-decade tracer study of the circulation and spreading rates of Atlantic water in the Arctic Ocean. *Journal of Geophysical Research: Oceans*, *129*(12), e2023JC020738. https://doi.org/10.1029/2023JC020738

Pavia, F. J., Anderson, R., Vivancos, S., Fleisher, M., Lam, P., Lu, Y., et al. (2018). Intense hydrothermal scavenging of 230Th and 231Pa in the deep Southeast Pacific. *Marine Chemistry*, *201*, 212–228. https://doi.org/10.1016/j.marchem.2017.08.003

Pavia, F. J., Anderson, R. F., Black, E. E., Kipp, L. E., Vivancos, S. M., Fleisher, M. Q., et al. (2019). Timescales of hydrothermal scavenging in the south Pacific Ocean from 234Th, 230Th, and 228Th. *Earth and Planetary Science Letters*, *506*, 146–156. https://doi.org/10.1016/j.epsl.2018.10.038

Pernov, J. B., Beddows, D., Thomas, D. C., Dall´Osto, M., Harrison, R. M., Schmale, J., et al. (2022). Increased aerosol concentrations in the High Arctic attributable to changing atmospheric transport patterns. *Npj Climate and Atmospheric Science*, *5*(1), 1–13. https://doi.org/10.1038/s41612-022-00286-y

Pfirman, S., Haxby, W. F., Colony, R., & Rigor, I. (2004). Variability in Arctic sea ice drift. *Geophysical Research Letters*, *31*(16), L16402. https://doi.org/10.1029/2004GL020063

Pickart, R. S., Weingartner, T. J., Pratt, L. J., Zimmermann, S., & Torres, D. J. (2005). Flow of winter-transformed Pacific water into the western arctic. *Deep Sea Research Part II: Topical Studies in Oceanography*, *52*(24), 3175–3198. https://doi.org/10.1016/j.dsr2.2005.10.009

Pokrovsky, O. S., Reynolds, B. C., Prokushkin, A. S., Schott, J., & Viers, J. (2013). Silicon isotope variations in Central Siberian rivers during basalt weathering in permafrost-dominated larch forests. *Chemical Geology*, *355*, 103–116. https://doi.org/10.1016/j.chemgeo.2013.07.016

Polyakov, I. V., Pnyushkov, A. V., Alkire, M. B., Ashik, I. M., Baumann, T. M., Carmack, E. C., et al. (2017). Greater role for Atlantic inflows on sea-ice loss in the Eurasian Basin of the Arctic Ocean. *Science*, *356*(6335), 285–291. https://doi.org/10.1126/science.aai8204

Polyakov, I. V., Rippeth, T. P., Fer, I., Alkire, M. B., Baumann, T. M., Carmack, E. C., et al. (2020). Weakening of cold halocline layer exposes sea ice to oceanic heat in the eastern Arctic Ocean. *Journal of Climate*, *33*(18), 8107–8123. https://doi.org/10.1175/JCLI-D-19-0976.1

Proshutinsky, A. Y., & Johnson, M. A. (1997). Two circulation regimes of the wind-driven Arctic Ocean. *Journal of Geophysical Research*, *102*(C6), 12493–12514. https://doi.org/10.1029/97JC00738

Proshutinsky, A. Y., Krishfield, R., Toole, J. M., Timmermans, M.-L., Williams, W., Zimmermann, S., et al. (2019). Analysis of the Beaufort gyre freshwater content in 2003–2018. *Journal of Geophysical Research: Oceans*, *124*(12), 9658–9689. https://doi.org/10.1029/2019JC015281

Rainville, L., & Woodgate, R. A. (2009). Observations of internal wave generation in the seasonally ice-free Arctic. *Geophysical Research Letters*, *36*(23), L23604. https://doi.org/10.1029/2009GL041291

Rampal, P., Weiss, J., & Marsan, D. (2009). Positive trend in the mean speed and deformation rate of Arctic sea ice, 1979–2007. *Journal of Geophysical Research*, *114*(C5), C05013. https://doi.org/10.1029/2008JC005066

Rantanen, M., Karpechko, A. Y., Lipponen, A., Nordling, K., Hyvärinen, O., Ruosteenoja, K., et al. (2022). The Arctic has warmed nearly four times faster than the globe since 1979. *Communications Earth & Environment*, *3*(1), 1–10. https://doi.org/10.1038/s43247-022-00498-3

Reynolds, B. C., Frank, M., & Halliday, A. N. (2006). Silicon isotope fractionation during nutrient utilization in the North Pacific. *Earth and Planetary Science Letters*, *244*(1), 431–443. https://doi.org/10.1016/j.epsl.2006.02.002

Richon, C., & Tagliabue, A. (2019). Insights into the major processes driving the global distribution of copper in the ocean from a global model. *Global Biogeochemical Cycles*, *33*(12), 1594–1610. https://doi.org/10.1029/2019GB006280

Roberts, H. M., & Shiller, A. M. (2015). Determination of dissolved methane in natural waters using headspace analysis with cavity ring-down spectroscopy. *Analytica Chimica Acta*, *856*, 68–73. https://doi.org/10.1016/j.aca.2014.10.058

Rudels, B., Jones, E. P., Anderson, L. G., & Kattner, G. (1994). On the intermediate depth waters of the Arctic Ocean. In *The Polar Oceans and Their Role in Shaping the Global Environment* (pp. 33–46). American Geophysical Union (AGU). https://doi.org/10.1029/GM085p0033

Rudels, B., Meyer, R., Fahrbach, E., Ivanov, V. V., Østerhus, S., Quadfasel, D., et al. (2000). Water mass distribution in Fram Strait and over the Yermak plateau in summer 1997. *Annales Geophysicae*, *18*(6), 687–705. https://doi.org/10.1007/s00585-000-0687-5

Saito, M. A., Noble, A. E., Hawco, N., Twining, B. S., Ohnemus, D. C., John, S. G., et al. (2017). The acceleration of dissolved cobalt's ecological stoichiometry due to biological uptake, remineralization, and scavenging in the Atlantic Ocean. *Biogeosciences*, *14*(20), 4637–4662. https://doi.org/10.5194/bg-14-4637-2017

Schauer, U., Loeng, H., Rudels, B., Ozhigin, V. K., & Dieck, W. (2002). Atlantic water flow through the Barents and Kara seas. *Deep Sea Research Part I: Oceanographic Research Papers*, *49*(12), 2281–2298. https://doi.org/10.1016/S0967-0637(02)00125-5

Schauer, U., Muench, R. D., Rudels, B., & Timokhov, L. (1997). Impact of eastern Arctic shelf waters on the Nansen Basin intermediate layers. *Journal of Geophysical Research*, *102*(C2), 3371–3382. https://doi.org/10.1029/96JC03366

Schlosser, P., Bayer, R., Bönisch, G., Cooper, L. W., Ekwurzel, B., Jenkins, W. J., et al. (1999). Pathways and mean residence times of dissolved pollutants in the ocean derived from transient tracers and stable isotopes. *Science of the Total Environment*, *237–238*, 15–30. https://doi.org/10.1016/S0048-9697(99)00121-7

Schlosser, P., Koffman, T., Newton, R., & Pasqualini, A. (2023). Data report tritium and helium isotopes: 2015 U.S. GEOTRACES arctic cruise GN01 (HLY1502), Version 1.0 [Dataset]. *Interdisciplinary Earth Data Alliance (IEDA)*. https://doi.org/10.26022/IEDA/112990

Schuur, E. A. G., Bockheim, J., Canadell, J. G., Euskirchen, E., Field, C. B., Goryachkin, S. V., et al. (2008). Vulnerability of permafrost carbon to climate change: Implications for the global carbon cycle. *BioScience*, *58*(8), 701–714. https://doi.org/10.1641/B580807

Serreze, M. C., Barrett, A. P., Slater, A. G., Woodgate, R. A., Aagaard, K., Lammers, R. B., et al. (2006). The large-scale freshwater cycle of the Arctic. *Journal of Geophysical Research*, *111*(C11), C11010. https://doi.org/10.1029/2005JC003424

Serreze, M. C., Barrett, A. P., Stroeve, J. C., Kindig, D. N., & Holland, M. M. (2009). The emergence of surface-based Arctic amplification. *The Cryosphere*, *3*(1), 11–19. https://doi.org/10.5194/tc-3-11-2009

Shiller, A. M., & Bairamadgi, G. R. (2006). Dissolved gallium in the northwest Pacific and the south and central Atlantic Oceans: Implications for aeolian Fe input and a reconsideration of profiles. *Geochemistry, Geophysics, Geosystems*, *7*(8), 2005GC001118. https://doi.org/10.1029/2005GC001118

Shimada, K., Itoh, M., Nishino, S., McLaughlin, F., Carmack, E., & Proshutinsky, A. (2005). Halocline structure in the Canada Basin of the Arctic Ocean. *Geophysical Research Letters*, *32*(3). https://doi.org/10.1029/2004GL021358

Shimada, K., McLaughlin, F., Carmack, E., Proshutinsky, A., Nishino, S., & Itoh, M. (2004). Penetration of the 1990s warm temperature anomaly of Atlantic water in the Canada basin. *Geophysical Research Letters*, *31*(20), 2004GL020860. https://doi.org/10.1029/2004GL020860

Simpson, K. G., Tremblay, J.-É., Gratton, Y., & Price, N. M. (2008). An annual study of inorganic and organic nitrogen and phosphorus and silicic acid in the southeastern Beaufort Sea. *Journal of Geophysical Research*, *113*(C7), C07016. https://doi.org/10.1029/2007JC004462

Smethie, W. M., Jr., Schlosser, P., Bönisch, G., & Hopkins, T. S. (2000). Renewal and circulation of intermediate waters in the Canadian Basin observed on the SCICEX 96 cruise. *Journal of Geophysical Research*, *105*(C1), 1105–1121. https://doi.org/10.1029/1999JC900233

Smethie, W. M., & Swift, J. H. (2018). Distribution of CFCs and SF6 measured on the 2015 GEOTRACES and repeat hydrography cruises to the Arctic Ocean. In *Presented at the Ocean Sciences Meeting*.

Spall, M. A., Pickart, R. S., Fratantoni, P. S., & Plueddemann, A. J. (2008). Western Arctic shelfbreak eddies: Formation and transport. *Journal of Physical Oceanography*, *38*(8), 1644–1668. https://doi.org/10.1175/2007jpo3829.1

Springer, A. M., & McRoy, C. P. (1993). The paradox of pelagic food webs in the northern Bering Sea—III. Patterns of primary production. *Continental Shelf Research*, *13*(5), 575–599. https://doi.org/10.1016/0278-4343(93)90095-F

Steele, M., Morison, J., Ermold, W., Rigor, I., Ortmeyer, M., & Shimada, K. (2004). Circulation of summer Pacific halocline water in the Arctic Ocean. *Journal of Geophysical Research*, *109*(C2), C02027. https://doi.org/10.1029/2003JC002009

Stroeve, J. C., Notz, D., Dawson, J., Schuur, E. A. G., Dahl-Jensen, D., & Giesse, C. (2025). Disappearing landscapes: The Arctic at +2.7°C global warming. *Science*, *387*(6734), 616–621. https://doi.org/10.1126/science.ads154

Swift, J. H., Kadko, D. C., Smethie, W. M., Becker, S. M., Barna, A., Cummiskey, J., et al. (2016). The Arctic Ocean then and now: Preliminary hydrographic data from the 2015 US GEOTRACES arctic expedition. In *Presented at the 2016 Ocean Sciences Meeting*.

Tank, S. E., McClelland, J. W., Spencer, R. G. M., Shiklomanov, A. I., Suslova, A., Moatar, F., et al. (2023). Recent trends in the chemistry of major northern rivers signal widespread Arctic change. *Nature Geoscience*, *16*(9), 789–796. https://doi.org/10.1038/s41561-023-01247-7

Taylor, J. R., Falkner, K. K., Schauer, U., & Meredith, M. (2003). Quantitative considerations of dissolved barium as a tracer in the Arctic Ocean. *Journal of Geophysical Research*, *108*(C12), 3374. https://doi.org/10.1029/2002JC001635

Taylor, R. L., Semeniuk, D. M., Payne, C. D., Zhou, J., Tremblay, J.-É., Cullen, J. T., & Maldonado, M. T. (2013). Colimitation by light, nitrate, and iron in the Beaufort Sea in late summer: Colimitation in the Beaufort Sea. *Journal of Geophysical Research: Oceans*, *118*(7), 3260–3277. https://doi.org/10.1002/jgrc.20244

Timmermans, M.-L., Proshutinsky, A., Golubeva, E., Jackson, J. M., Krishfield, R., McCall, M., et al. (2014). Mechanisms of Pacific summer water variability in the Arctic's Central Canada basin. *Journal of Geophysical Research: Oceans*, *119*(11), 7523–7548. https://doi.org/10.1002/2014JC010273

Timmermans, M.-L., Toole, J., Krishfield, R., & Winsor, P. (2008). Ice-Tethered Profiler observations of the double-diffusive staircase in the Canada Basin thermocline. *Journal of Geophysical Research*, *113*(C1), C00A02. https://doi.org/10.1029/2008JC004829

Toyoda, S., Kakimoto, T., Kudo, K., Yoshida, N., Sasano, D., Kosugi, N., et al. (2021). Distribution and production mechanisms of N2O in the western Arctic Ocean. *Global Biogeochemical Cycles*, *35*(4), e2020GB006881. https://doi.org/10.1029/2020GB006881

Tremblay, J.-É., Anderson, L. G., Matrai, P., Coupel, P., Bélanger, S., Michel, C., & Reigstad, M. (2015). Global and regional drivers of nutrient supply, primary production and CO_2 drawdown in the changing Arctic Ocean. *Progress in Oceanography*, *139*, 171–196. https://doi.org/10.1016/j.pocean.2015.08.009

Tremblay, J.-É., Raimbault, P., Garcia, N., Lansard, B., Babin, M., & Gagnon, J. (2014). Impact of river discharge, upwelling and vertical mixing on the nutrient loading and productivity of the Canadian Beaufort Shelf. *Biogeosciences*, *11*(17), 4853–4868. https://doi.org/10.5194/bg-11-4853-2014

Twining, B., Morton, P., & Salters, V. (2019). Trace element concentrations (labile and total measurements) in particles collected with GO-Flo bottles and analyzed with ICP-MS from the US GEOTRACES Arctic cruise (HLY1502; GN01) from August to October 2015 [Dataset]. *Biological and Chemical Oceanography Data Management Office*. https://doi.org/10.1575/1912/bco-dmo.771474.2

van Ooijen, J. C., Rijkenberg, M. J. A., Gerringa, L. J. A., Rabe, B., & Rutgers van der Loeff, M. M. (2016). Inorganic nutrients measured on water bottle samples during POLARSTERN cruise PS94 (ARK-XXIX/3) [Dataset]. *Royal Netherlands Institute for Sea Research, Texel, PANGAEA*. https://doi.org/10.1594/PANGAEA.868396

Varela, D. E., Brzezinski, M. A., Beucher, C. P., Jones, J. L., Giesbrecht, K. E., Lansard, B., & Mucci, A. (2016). Heavy silicon isotopic composition of silicic acid and biogenic silica in Arctic waters over the Beaufort shelf and the Canada Basin. *Global Biogeochemical Cycles*, *30*(6), 804–824. https://doi.org/10.1002/2015GB005277

Vieira, L. H., Achterberg, E. P., Scholten, J., Beck, A. J., Liebetrau, V., Mills, M. M., & Arrigo, K. R. (2019). Benthic fluxes of trace metals in the Chukchi Sea and their transport into the Arctic Ocean. *Marine Chemistry*, *208*, 43–55. https://doi.org/10.1016/j.marchem.2018.11.001

Villalobos, M., Bargar, J., & Sposito, G. (2005). Mechanisms of Pb(II) sorption on a biogenic manganese oxide. *Environmental Science and Technology*, *39*(2), 569–576. https://doi.org/10.1021/es049434a

Walsh, J. J., Dieterle, D. A., Maslowski, W., Grebmeier, J. M., Whitledge, T. E., Flint, M., et al. (2005). A numerical model of seasonal primary production within the Chukchi/Beaufort Seas. *Deep Sea Research Part II: Topical Studies in Oceanography*, *52*(24), 3541–3576. https://doi.org/10.1016/j.dsr2.2005.09.009

Walvoord, M. A., Voss, C. I., & Wellman, T. P. (2012). Influence of permafrost distribution on groundwater flow in the context of climate-driven permafrost thaw: Example from Yukon Flats basin, Alaska, United States: Permafrost distribution and groundwater flow. *Water Resources Research*, *48*(7), W07524. https://doi.org/10.1029/2011WR011595

Weingartner, T. J., Cavalieri, D. J., Aagaard, K., & Sasaki, Y. (1998). Circulation, dense water formation, and outflow on the northeast Chukchi Shelf. *Journal of Geophysical Research*, *103*(C4), 7647–7661. https://doi.org/10.1029/98JC00374

Weiss, W., & Roether, W. (1980). The rates of tritium input to the world oceans. *Earth and Planetary Science Letters*, *49*(2), 435–446. https://doi.org/10.1016/0012-821X(80)90084-9

Whitmore, L., & Shiller, A. M. (2024). Dissolved methane (CH_4) concentrations from the U.S. GEOTRACES arctic cruise (HLY1502; GN01) on USCGC healy from August to October 2015 [Dataset] (Version 1) Version Date 2024-12-20. *Biological and Chemical Oceanography Data Management Office (BCO-DMO)*. https://doi.org/10.26008/1912/bco-dmo.946112.1

Whitmore, L. M., Morton, P. L., Twining, B. S., & Shiller, A. M. (2019). Vanadium cycling in the Western Arctic Ocean is influenced by shelf-basin connectivity. *Marine Chemistry*, *216*, 103701. https://doi.org/10.1016/j.marchem.2019.103701

Whitmore, L. M., Pasqualini, A., Newton, R., & Shiller, A. M. (2020). Gallium: A new tracer of Pacific water in the Arctic Ocean. *Journal of Geophysical Research: Oceans*, *125*(7), e2019JC015842. https://doi.org/10.1029/2019JC015842

Whitmore, L. M., & Shiller, A. M. (2016). *Distribution and flux of methane in the 2015 U.S. GEOTRACES Arctic section* (Vol. 3408). Goldschmidt Abstracts. Retrieved from https://goldschmidtabstracts.info/abstracts/abstractView?id=2016001891

Whitmore, L. M., Shiller, A. M., Horner, T. J., Xiang, Y., Auro, M. E., Bauch, D., et al. (2022). Strong margin influence on the Arctic Ocean barium cycle revealed by Pan-arctic synthesis. *Journal of Geophysical Research: Oceans*, *127*(4), e2021JC017417. https://doi.org/10.1029/2021JC017417

Wolgemuth, K., & Broecker, W. S. (1970). Barium in sea water. *Earth and Planetary Science Letters*, *8*(5), 372–378. https://doi.org/10.1016/0012-821X(70)90110-X

Woodgate, R. A., Aagaard, K., Swift, J. H., Falkner, K. K., & Smethie, W. M. (2005). Pacific ventilation of the Arctic Ocean's lower halocline by upwelling and diapycnal mixing over the continental margin: Pacific diapycnal halocline ventilation. *Geophysical Research Letters*, *32*(18). https://doi.org/10.1029/2005GL023999

Woodgate, R. A., Aagaard, K., & Weingartner, T. J. (2005). A year in the physical oceanography of the Chukchi Sea: Moored measurements from autumn 1990–1991. *Deep Sea Research Part II: Topical Studies in Oceanography*, *52*(24–26), 3116–3149. https://doi.org/10.1016/j.dsr2.2005.10.016

Woodgate, R. A., & Peralta-Ferriz, C. (2021). Warming and freshening of the Pacific inflow to the arctic from 1990-2019 implying dramatic shoaling in Pacific winter water ventilation of the arctic water column. *Geophysical Research Letters*, *48*(9), e2021GL092528. https://doi.org/10.1029/2021GL092528

Woosley, R. J., & Millero, F. J. (2020). Freshening of the western Arctic negates anthropogenic carbon uptake potential. *Limnology & Oceanography*, *65*(8), 1834–1846. https://doi.org/10.1002/lno.11421

Xiang, Y., & Lam, P. J. (2020). Size-fractionated marine suspended particle dynamics in the Western Arctic Ocean: Lateral and vertical sources. *Journal of Geophysical Research: Oceans*, *125*(8), e2020JC016144. https://doi.org/10.1029/2020jc016144

Xiang, Y., Lam, P. J., Burd, A. B., & Hayes, C. T. (2022). Estimating mass flux from size-fractionated filtered particles: Insights into controls on sinking Velocities and mass fluxes in recent U.S. GEOTRACES cruises. *Global Biogeochemical Cycles*, *36*(4), e2021GB007292. https://doi.org/10.1029/2021GB007292

Xiang, Y., Lam, P. J., & Lee, J. M. (2021). Diel redox cycle of manganese in the surface Arctic Ocean. *Geophysical Research Letters*, *48*(23), e2021GL094805. https://doi.org/10.1029/2021GL094805

Yamamoto-Kawai, M., McLaughlin, F. A., Carmack, E. C., Nishino, S., Shimada, K., & Kurita, N. (2009). Surface freshening of the Canada Basin, 2003–2007: River runoff versus sea ice meltwater. *Journal of Geophysical Research*, *114*(C1), C00A05. https://doi.org/10.1029/2008JC005000

Zhang, R., Jensen, L. T., Fitzsimmons, J., Sherrell, R. M., Lam, P., Xiang, Y., & John, S. (2021). Iron isotope biogeochemical cycling in the western Arctic Ocean. *Global Biogeochemical Cycles*, *35*(11), e2021GB006977. https://doi.org/10.1029/2021GB006977

Zhang, R., Jensen, L. T., Fitzsimmons, J. N., Sherrell, R. M., & John, S. (2019). Dissolved cadmium and cadmium stable isotopes in the western Arctic Ocean. *Geochimica et Cosmochimica Acta*, *258*, 258–273. https://doi.org/10.1016/j.gca.2019.05.028

Zhuang, Y., Jin, H., Cai, W.-J., Li, H., Qi, D., & Chen, J. (2022). Extreme nitrate deficits in the western Arctic Ocean: Origin, decadal changes, and implications for denitrification on a polar marginal shelf. *Global Biogeochemical Cycles*, *36*(7), e2022GB007304. https://doi.org/10.1029/2022gb007304